

# Stability of the Sikorsky S-76 Bearingless Main Rotor

James M. Wang  
Dynamicist

James Duh  
Dynamicist

Jon-Shen Fuh  
Dynamicist

Sikorsky Aircraft Division  
United Technologies Corporation  
Stratford, CT

Sesi Kottapalli  
Dynamicist

Rotorcraft Aeromechanics Branch  
NASA Ames Research Center  
Moffett Field, CA

The stability results of an extensive wind tunnel test of the Sikorsky proof-of-concept 5-bladed full-scaled bearingless main rotor are presented. The test was conducted in 1992 at the NASA Ames 40x80 wind tunnel. All five blade flexbeams were instrumented with edgewise and flapwise strain gauges. This provided a rare opportunity to compare BMR stability in both rotating and fixed reference frame, and to check for blade-to-blade dissimilarities. Analytical predictions are also included to demonstrate that stability can be predicted reasonably well. The effect of nonlinear damping characteristics are also shown. Furthermore, this paper reveals an experimental study of how the lag mode stability differs among the different lag modes (i.e. regressing, progressing, and collective).

## INTRODUCTION

In recent years there has been a growing interest in bearingless rotors because of design simplicity, easier maintenance, suitability to aeroelastic tailoring, improved handling qualities, and extended fatigue life. In a bearingless rotor the flap and lag hinges, as well as the pitch bearings, have all been replaced by a torsionally soft flexbeam between the blade and the hub (Figs. 1 and 2). Pitch control is applied to the blade through a torsionally stiff torque tube by rotating the tube with a pushrod. The torque tube in turn twists the flexbeam. To achieve manageable edgewise bending stress on the flexbeam, bearingless rotors are usually designed as soft-inplane rotors. However, soft-inplane rotors may be subjected to unfavorable

bending-torsion coupling, and the low frequency regressing lag mode may coalesce with the fuselage modes to cause air or ground resonance instability. For articulated rotors, the instability problems are taken care of by adding mechanical lag dampers. Since there is no lag hinge on bearingless rotors, traditional lag damper can not be effectively used.

A distinguishing feature of the Sikorsky 5-bladed BMR is the snubber/damper located at the inboard end of the flexbeam (Fig. 2). The snubber/damper serves many purposes: the snubber portion provides a pivoting point for the inboard end of the torque tube and prevents excessive static droop, the damper portion functions as a lead-lag damper and introduces negative pitch-lag coupling (lag-back nose-up) to increase lag mode aerodynamic damping. This snubber/damper must be analytically modeled properly to predict the rotor stability.

The Sikorsky proof-of-concept BMR has a 44 ft diameter and is sized for the Sikorsky S-76

---

*Presented at the American Helicopter Society  
49th Annual Forum, St Louis, Missouri, May 19-  
21, 1993. Copyright © 1993 by the American  
Helicopter Society, Inc. All rights reserved.*

helicopter. The full-scale wind tunnel test examined the rotor shaft-fixed stability, vibratory hub loads, acoustics, stress and strains, handling qualities, and performance. The test included flight conditions from 0 to 200 knots, and thrust level of -4,000 to 18,000 lbs. A detailed description of the test program can be found in Ref. [1]. Parametric sweeps were conducted to systematically examine the effects of rotor speed, forward speed, thrust level, cyclic pitch, shaft tilt, and higher harmonic controls [2] on BMR loads and stability. The test has provided a comprehensive set of data for better understanding of the bearingless rotor and for assessing the state-of-the-art of BMR analyses.

## DESCRIPTION OF THE EXPERIMENT

The full-scaled rotor experiment was performed at the NASA Ames 40 by 80 Foot Wind Tunnel of the National Full-Scale Aerodynamic Complex (NFAC). The rotor (Fig. 1) was mounted on NASA's rotor test apparatus (RTA). The RTA fuselage contains two 1,500 h.p. electric drive motors, a hydraulic actuator system, and a five component balance that measures three forces and two moments. The RTA fuselage sits on three struts. The entire RTA fuselage can tilt forward or aft to change the rotor shaft angle. The fuselage was not gimballed, hence, it was an isolated rotor stability test. The rotor plane was 21.5 feet above the tunnel floor.

Dynamic inputs to excite the rotor system were provided by oscillating the three stationary pushrods which support the swashplate. The stationary pushrods were each attached to a camed lever which could rotate to oscillate the blade approximately +/- 1 deg from 0 to 40 Hz (Fig. 2). To excite the regressing lag mode, the input to the cam actuators are phased to cause a nutation of the swashplate at the regressing lag frequency. The dynamic actuators were also used to provide Chirp excitations to help determine the rotor modal frequencies, and for higher harmonic control studies.

For soft-inplane bearingless rotors, the weakly-damped first lag mode is the most susceptible to aeroelastic instability. Therefore, the objective of the stability test was to determine the lag mode damping under various flight conditions. The 1G

condition for the S-76 rotor is 10,500 lbs of thrust. The nominal rotor speed (100% Nr) is at 315 rpm. Stability data were obtained for the following test conditions:

- Hover collective pitch sweep from 0.7° to 11.7°, at 1° increment.
- Hover rotor speed sweep from 283 to 346 rpm.
- Forward flight at 10,500 lbs from 0 to 200 knots.
- Forward flight at 14,000 lbs from 0 to 160 knots.
- Forward flight at 16,000 lbs from 0 to 140 knots.
- Thrust sweep at 80 knots from -1,835 to 15,700 lbs.
- Thrust sweep at 120 knots from -4,000 to 15,500 lbs.
- Shaft angle sweep at 80 knots from +5 to -10 degrees.
- Rotor speed sweep at 160 knots, from 285 to 315 rpm.
- B1S cyclic sweep at hover and at 120 knots.

The test procedure was to trim the rotor to the shaft angle and hub forces and moments predicted by Sikorsky's GenHel (General Helicopter) trim program. The swashplate was then nutated at the regressing lag frequency. After the rotor reached a steady state, the excitation was cut off, and the transient was recorded for 8 seconds at a sampling rate of 128 points per second. This generated a total of 1024 points for each test condition. A total of 16 data channels were recorded. They include lead-lag response at the 4.5% radius for all five flexbeams, snubber displacement, rotating pushrod load, flapwise response at the 4.5% radius, balance side force, and the dynamic actuators time history.

For the lead-lag signals, they can be examined individually in the rotating frame, or summed up via multiblade coordinate transformation (MCT) to obtain the rotor response in the fixed reference frame. From the rotating frame, or fixed frame decaying transient signal, the frequency spectrum was determined using a Fast Fourier Transform, then a Moving Block technique was used to estimate the lag mode damping.

## ANALYTICAL METHODOLOGIES

The analysis of a bearingless rotor system is more involved than that of a hingeless, or

articulated rotor system because of the redundant load path through the torque tube, and the modeling of the snubber/damper assembly. In addition, bearingless rotors achieve pitch change through elastically twisting and bending of the flexbeam, thus bending-torsion coupling must be treated in a more careful manner. There have been many studies on the aeroelastic stability of hingeless rotors. However, limited analytical work has been done to examine the aeroelastic stability of bearingless rotors. Due to redundant load path and nonlinear structural couplings, routinely used methods of modeling the hingeless rotor with rigid blade and spring at the equivalent hinge offset have to be exercised carefully with good engineering judgement.

Most of the previous theoretical work on bearingless rotor have been limited to hover because forward flight complicates the analysis by requiring solving nonlinear equations with periodic coefficients. Furthermore, in forward flight the aeroelastic problem is coupled to the trim state of the helicopter, thus, both the nonlinear blade response and nonlinear trim equations need to be solved simultaneously. Three computer programs were employed for the stability predictions described in this paper. They are Sikorsky's HELSA, RDYNE, and Sikorsky version of the University of Maryland Advanced Rotorcraft Code (UMARC/S). A brief description of each program follows.

### HELSA

The Helicopter Stability Analysis (HELSA) [3] was developed by Sikorsky Aircraft to predict coupled rotor/body or isolated rotor stability in hover. The analysis includes coupled elastic flap, lag and torsion modes, and elastic or rigid airframe modes. The perturbation equations of motion are derived about an equilibrium state, and terms up to 2nd order are retained for blade displacement, and 3rd order for blade torsion. Blade element theory and airfoil table lookup are used for aerodynamic calculations. Airframe modes are imported from outside of the code. Periodic coefficients are eliminated by transforming the coupled blade/fuselage equations into the nonrotating frame, and then solved via an eigen analysis.

### RDYNE

RDYNE (Rotorcraft Dynamics Analysis) [4,5,6] is a comprehensive rotor trim/time history program developed at Sikorsky. Solution is obtained by a time-marching procedure. The integrated time responses are post-processed to obtain the hub loads, frequency content, and rotor stability. Quasi-steady blade element theory and unsteady aerodynamic modeling are used. Variable rotor induced inflow is accounted for by geometric influence coefficients derived from a prescribed or free wake pre-processor. Control may be varied with time to simulate a control input, or lag damper coefficient may be varied with lag velocity to approximate a nonlinear lag damper. A restart capability is used to change inputs to simulate, for example, pushrod failure, or to provide for low-cost calculations of changes in a design parameter such as blade weight or stiffness. A prescribed blade displacement capability may be used to find rotor loads in a maneuver or for correlation studies [6]. Recently, a new version of RDYNE [4] has been developed which uses coupled blade modes for the representation of BMR with redundant load paths.

### UMARC/S

The Sikorsky version of UMARC/S [7-11] is used for calculating the blade natural frequencies and for examining the S-76 BMR stability. The code has been carefully modified to include the Sikorsky BMR and snubber/damper kinematics. The snubber/damper is modeled as equivalent springs and dampers. The springs and dampers can rotate with the torque tube and interact properly with the pitch link to give lag-flap-pitch coupling.

The analysis in forward flight consists of two phases: (1) calculation of the steady state rotor response and vehicle trim controls, and (2) calculating the stability of the coupled rotor-body system.

The analysis is based on a finite element method in space and time. The blade is assumed as an elastic beam undergoing flap bending, lead-lag bending, elastic twist, and axial extension. This Bernoulli-Euler beam is allowed small strains, and moderate deflections. Due to the moderate deflection assumption, the equations contain nonlinear structure, inertia and aerodynamic

terms. The blade is discretized into a number of beam elements. For a BMR rotor a number of elements are used for modeling the blade, some for the flexbeam, and the remaining elements are for the torque tube. Each element has fifteen degrees of freedom. Between elements there is a continuity of displacement and slope. The boundary conditions are formulated to accept articulated, hingeless, or bearingless rotors. The fuselage is modeled as a rigid body with three translational and two rotational degrees of freedom. The rotor aerodynamic loads are based on quasi-steady strip theory. Linear unsteady aerodynamic modeling, trailing edge separation, and dynamic stall have been included to improve the response prediction. Dynamic inflow modeling is added during stability calculation to capture the low frequency unsteadiness due to shed wakes.

The rotor response calculation is iterated until the desired steady-state thrust is reached and the forces and moments on the aircraft reach an equilibrium, the nonlinear blade equations are then linearized about the equilibrium blade response to obtain the perturbation equations for each blade. To reduce computation time, the resulting perturbation equations are transformed into normal mode domain using the coupled free vibration characteristics of the blade about the mean deflected position. These perturbation equations, along with the dynamic inflow equations and coupled blade/fuselage equations are transformed to the fixed reference frame via the multiblade coordinate transformation. In hover, the stability roots are obtained via conventional eigen analysis of matrix with constant coefficients. For forward flight analysis, periodic coefficients arise from cyclically varying aerodynamic loads across the rotor disk. Floquet theory is used to obtain the stability of the periodic system.

## RESULTS AND DISCUSSION

### Frequency Correlation

Rotor frequency placement is one of the many important parameters that influence aeromechanical stability. A successful prediction of the rotor frequencies implies a good modeling of the structural properties and the

snubber/damper kinematics. The measured and predicted frequencies for this BMR is shown in Fig. 3. The nonrotating frequencies were obtained from a static shake test of the blade. The static shake test also gave valuable information on the nonlinear modal damping behaviors of the snubber/damper, and blade mode shapes. The rotating frequencies were monitored online with an HP 3562 spectrum analyzer, and measured via the following three techniques.

(1) Swashplate Cyclic Excitation The swashplate was shaken in the fixed frame with the number 3 dynamic actuator (D3) from 0 to 40 Hz at 0.5 Hz increment. In order to save valuable wind tunnel time, the rotor was only shaken at frequencies near the existence of a mode. This single actuator produced a mixture of collective and cyclic inputs. Shaking the rotor in the fixed frame at a frequency  $\omega$  generates an  $\omega+1/\text{rev}$  and an  $\omega-1/\text{rev}$  excitations in the rotating frame. The flapwise, edgewise, and torsional responses at these two excitation frequencies were plotted versus frequency to yield the blade frequency response function. Figure 4 illustrates the edgewise frequency response function measured at the nominal rotor speed, 315 rpm. The hollow squares represent the  $\omega-1/\text{rev}$  response, and the solid squares represent the  $\omega+1/\text{rev}$  response. The first and second lag modes are clearly seen at 3.8 Hz and 25 Hz, respectively.

(2) N-per-rev Frequency Crossing This technique was also used to find the rotating frame blade frequencies. This technique makes use of the resonance phenomenon. When a blade mode frequency coalesces with a N-per-rev forcing frequency, the blade response for that particular mode is amplified. This technique requires no artificial input to excite the system. It only requires sweeping the rotor rpm. It utilizes existing aerodynamic turbulence in the tunnel to generate the N-per-rev excitation. After the test, the 1P, 2P, 3P, up to 10P responses of the flapwise and edgewise strain gauges were plotted versus rotor speed. If a resonance peak appears on the plot, then it implies that there is a frequency coalescence, or a blade mode, at that rotor speed. The advantage of this technique is that it is a fast way to obtain the blade modes for a wide rpm range. The drawback is that it requires fine rpm increments (around 5 rpms) to pick out the peaks confidently. Figure 5 shows

the 5P edgewise response vs. rotor speed measured at 40, 60 and 80 knots (note, the rotor thrusts are different). The peak at 285 rpm is the 2nd lag mode. The 40 and 80 knots cases capture the 2L peak clearly, but the 60 knots case does not show a coalescence.

(3) Swashplate Chirp Excitation Chirp inputs have been used routinely in flight tests, but this is the first time that Chirp has been used in a wind tunnel test. Chirp is a time-varying sinusoidal signal. A 0.8 to 12 Hz Chirp that lasted 70 seconds was used to excite the low frequency rotor modes. A 10 to 40 Hz Chirp was used to excite the high frequency modes. A random noise with a standard deviation equals to half the Chirp amplitude was summed in to reduce the coherence of the non-cross talk channel. A notch filter was also added at the 1P frequency to reduce the 1/rev influence.

The time histories from the edgewise and flapwise strain gauges of all five flexbeams were transformed to the fixed frame using MCT, and then examined using the CIFER system identification program [12]. The MCT procedure used is defined as follows:

$$\zeta_0(t) = \frac{1}{N_b} \sum_{m=1}^{N_b} \zeta_m(\psi_m)$$

$$\zeta_{1c}(t) = \frac{2}{N_b} \sum_{m=1}^{N_b} \zeta_m(\psi_m) \cos(\psi_m)$$

$$\zeta_{1s}(t) = \frac{2}{N_b} \sum_{m=1}^{N_b} \zeta_m(\psi_m) \sin(\psi_m)$$

$$\zeta_{2c}(t) = \frac{2}{N_b} \sum_{m=1}^{N_b} \zeta_m(\psi_m) \cos(2\psi_m)$$

$$\zeta_{2s}(t) = \frac{2}{N_b} \sum_{m=1}^{N_b} \zeta_m(\psi_m) \sin(2\psi_m)$$

where,  $\zeta_m(\psi_m) = EB12_m(t)$ , the response from the #12 edgewise strain gauge which was

mounted at the 4.5% radial location on flexbeam for the m-th blade.

Figures 6 and 7 present the cosine lag ( $\zeta_{1c}$ ) and collective lag ( $\zeta_0$ ) frequency response functions from a 0.8 to 12 Hz Chirp excitation. Figure 6 shows that the regressing lag mode is at 1.6 Hz. Figure 6 shows, for the first time, the 2nd regressing of the first lag mode (1L2reg), and the 2nd progressing of the first lag mode (1L2prog), and the 2nd regressing of the second lag mode (2L2reg) all have been identified experimentally. This is only possible because all five blades were instrumented.

Figure 7 shows that the collective lag mode is at 2.7 Hz. However, Fig. 4 shows the rotating frame lag frequency is 3.8 Hz (0.7/rev). The collective lag frequency is less than 3.8 Hz due to a coupling between the transmission and collective lag. The flap mode frequencies are more difficult to identify because they are heavily damped and masked by the strong 1/rev peak.

### Lag Mode Stability

The S-76 BMR was found to be stable at all test conditions. Measured damping generally follows the UMARC/S prediction quite well, around 4 to 5% at 14,000 lbs in hover and high airspeed, and 2 to 3% at the bucket airspeed (80 knots).

Over 200 stability data points were collected. Many of them are repeat points. Usually three stability data points were taken at each prescribed test condition. Occasionally, the same flight condition was repeated in another run just to check the repeatability and to check for continuity among different data sets. The damping values were reduced online using NASA's Moving Block software. The responses were also post-processed using Sikorsky's Moving Block program and NASA's time domain software; all three methods yield similar results.

In hover stability tests, the main rotor shaft was always tilted forward at 10 degrees, and the wind tunnel ceiling was open to minimize turbulence from recirculation. It was noticed that just from the forward tilt of the rotor, a 5 to 10 knots wind velocity was generated inside the wind tunnel.

In forward flight, two types of rotor trims were employed. One method was to adjust the longitudinal cyclic to obtain the propulsive force and moment that were necessary to overcome the hypothetical aircraft drag and down-loads of the horizontal tail stabilizer. This is generally referred to as propulsive trim, or H-force trim. The propulsive trim settings used during this test were predicted by Sikorsky's GenHel analysis using the flat plate drag area and horizontal tail stabilizer area for the Comanche fuselage.

A second trim method is to keep the shaft angle the same as the propulsive trim, but adjusts the cyclics to minimize longitudinal and lateral flappings. This is referred to as wind tunnel trim.

### Stability Data Quality

The quality of the log decrement line on the Moving Block depends on the amplitude of the regressing lag mode (3.8 Hz) relative to the 1P amplitude (5.25 Hz). These two are considered as "close modes." In hover, the Moving Block lines are clean, with very little 1P ripple, because the tip path plane is perpendicular to the rotor shaft. The minute 1P harmonic in the hover data is due to the 10 degrees forward shaft tilt which produces a cyclic load. In forward flight, if the rotor is trimmed to the Genhel propulsive force condition, then there is a strong rotor 1P. This adds large ripples to the Moving Block line and makes it difficult to decipher the lag damping. A least square fit line through the rippled Moving Block line gives reasonable damping estimation. Figures 8a and 8b show the difference in Moving Block line between hover, and a forward flight case at 120 knots.

This BMR with a snubber/damper as shown in Fig. 2, has nonlinear damping characteristics: for a small lag amplitude, the lag damping "increases" with lag amplitude. For large displacements, the snubber/damper damping is nearly constant. From the hover tests, or from the nonrotating blade pull tests, the Moving Block lines show a kink: a steep slope at the beginning, and a shallower slope later (Fig. 8a). This shows that lag mode damping is larger during the first portion of the transient decay, and as the lag amplitude diminishes, the damping drops.

Sometimes, there may exist two kinks: a large damping initially, then, a lower damping as lead-lag amplitude diminishes, finally, followed by a shallow curve with ripples due to the lead-lag motion becomes buried by the 1/rev lead-lag.

By picking different lengths of the Moving Block log decrement curve for curve fitting, a wide range of Moving Block damping value can exist. It requires user judgement to determine a "best fit." Therefore, the same user should process all the stability data in order to be consistent. In general, both the record length and window size should be adjusted according to each set of data. It is preferable to use as long a record length as possible to capture more of the signal, and then use as small a Moving Block window as possible to capture the nonlinear damping phenomenon.

Even though the different rotor lag modes (collective lag, regressing lag, or progressing lag) all have the same oscillatory frequency in the rotating frame, but their fixed frame frequencies are different [9]. Since the rotor was perturbed by exciting the swashplate in the nonrotating frame, post processings reveal that the "type" of lag mode that gets excited (collective lag, regressing lag, or progressing lag) mainly depends on the shake frequency. Post test studies have shown that it is not necessary to use nutation shaking. If the shake frequency is correct, then a pure longitudinal, or lateral, or collective, or any combination can excite the desired lag mode.

Test results have demonstrated that when the rotor was excited at the fixed frame regressing lag frequency, then the rotating frame decay rate measured from a "single" blade is almost identical to the true "rotor" regressing lag mode decay rate obtained by doing a multiblade coordinate transform. All stability data points presented in the following section are from the edgewise strain gauge at the 4.5% radius location of blade 1. The frequency and damping for all five blades were checked at the end of each run everyday. There is very little dissimilarities among the five blades.

During the test it was discovered that the regressing lag mode was more difficult to excite when the blade coning angle was small. When there is little coning, the flap-lag coupling due to flexbeam twist and Coriolis is weak. Then,

oscillating the blade pitch only causes the blade to flap up and down, and very little inplane motion is introduced. This suggests that instead of keeping the shaking amplitude the same for all stability testings, it maybe better to adjust the shaking amplitude, such that the excited lag amplitudes are same. But, sometimes this is not possible due to mechanical limitations. During this wind tunnel test, the criterion for setting the shake amplitude was to turn up the excitation to as high as possible until, either, the flexbeam DNE (do not exceed) value was reached, or the dynamic shaker travel limit was reached.

### Hover Stability

Figure 9 presents the damping for a collective pitch sweep in hover. At low collective pitch (below 5 deg), the measured damping is less than HELSA prediction. This is because a constant snubber damping value was used in the analysis, while the true spring stiffness and damping of the snubber/damper is nonlinear. For small displacements, the snubber/damper damping is proportional to displacement. If the snubber damping value has been adjusted in the calculation to match the snubber/damper amplitude, such as done in UMARC/S, then the prediction becomes very good (Fig. 9). The snubber displacement can be obtained from test data, or from response calculations.

Fig. 10 shows the effect of increasing longitudinal cyclic pitch on hover stability for 2 degrees collective. Figure 10 shows a steady increase in regressing lag damping with more cyclic. This is because adding cyclic increases 1P lead-lag motion through Coriolis coupling, which also increases the snubber/damper displacement amplitude. Hence, the snubber/damper works harder and provides more damping.

### Forward Flight Stability

Figures 11, 12, and 13 present the forward flight stability of the Sikorsky BMR at 10,500 lbs, 14,000 lbs and 16,000 lbs thrust conditions. The discrete points are experimental data. The solid line are analytical prediction done prior to the wind tunnel test. As shown in the figures, the pretest predictions correlate well with the

measured data. In the UMARC/S analysis, the six blade modes with the lowest frequency were used for modal normalization (1st lag, 1st flap, 2nd flap, 3rd flap, 2nd lag, 1st torsion and 4th flap). A 3-state Pitt and Peters dynamic inflow model [13] was also used. Even though this is a shaft-fixed rotor stability test, but there is always some flexibility in the test stand. The generalized mass and stiffness for the RTA stand pitch and roll degrees of freedom were obtained from a shake test. For a five bladed rotor, this yielded 67 states for the Floquet stability analysis. The Floquet eigenvalues were identified by examining the Floquet eigenvectors [9,10,11].

At each test point, the rotor was excited three times to collect three transient responses. In Fig. 12, data for both propulsive and wind tunnel trim are shown. Figure 12 shows propulsive trim gives slightly higher lag mode damping than wind tunnel trim. This is due to propulsive trim increases cyclic flapping, hence larger snubber/damper motion, therefore, more snubber damping.

The effect of cyclic flapping on lag mode damping in forward flight is illustrated in Fig. 14. The measured rotating frame dampings are plotted versus longitudinal cyclic pitch input. In Figs. 14 to 17 the dashed lines represent a curve fit of the data points. In both hover (Fig. 10) and forward flight (Fig. 14), increasing the 1P cyclic increases damping.

The effect of rotor thrust on lag mode damping at 80 knots is shown in Fig. 15. This figure illustrates that damping is proportional to aerodynamic thrust. This phenomenon is found on most shaft-fixed BMR and hingeless rotor tests [7]. Analysis shows the increase in lag damping is not due to an increase in flap damping. The increase is because at higher thrust the blade becomes more twisted, which then couples the inplane motion more with the flap motion.

The effect of rotor thrust on lag mode damping at 120 knots is shown in Fig. 16. The shape is similar to the 80-knot case. Notice the minimum damping point for both cases does not occur at zero thrust, it happens at two to three thousands pounds. This is probably due to the 2.5 degree flexbeam precone [7]. Without any precone, the lag stability curve usually is symmetrical about

the zero thrust point. In general, for an isolated rotor, when there is precone, the valley of the lag damping versus thrust (or collective) curve is shifted toward the right.

The effect of rotor shaft tilt angle on lag mode damping at 80 knots is shown in Fig. 17. If the tunnel speed, rotor speed, and collective pitch are constant, then a rearward shaft tilt produces more thrust than forward shaft tilt. To remove the effect of thrust change on damping, the collective pitch was adjusted at each shaft angle to yield a steady 14,000 lbs thrust. Figure 17 illustrates that even if the thrust is constant, changing the shaft angle can still affect lag mode damping.

Stability Differences Between Rotating and Fixed Frame Lag Modes

In Figs. 8 - 17, the damping values were obtained from the transient decay time history of blade number 1 only. However, the transient response in the rotating frame actually contains lag motion that gives rise to "rotor" collective, regressing, and progressing lag modes. To truly measure the regressing lag mode damping, the time history from all five blades should be summed up using multiblade coordinate transformation (MCT) to obtain the cosine or the sine lag component time history. Then, perform a FFT and Moving Block on either the cosine lag or sine lag time history to yield the true regressing lag frequency and damping in the nonrotating frame. Similarly, the collective lag frequency and damping can only be obtained by doing a MCT first to obtain the collective lag component time history, then perform a FFT and Moving Block analysis.

Figure 18 shows the lead-lag time history, FFT and Moving Block obtained in the rotating frame from a flexbeam strain gauge on blade 1 (FB1EB12). The gauge is at 4.5% radial position. The results are for a hover case with 2 degrees collective at 3/4 span (Run 9, Point 5). The peak at 3.84 Hz is the lag frequency measured in the rotating frame. In the rotating frame, it is not possible to determine whether the lag motion is a collective mode, progressing mode, or regressing mode, because the natural frequency is always at 3.84 Hz.

Figure 19 shows the time history for all five blades and the snubber displacement of blade 1 for Run 9, Point 5. The phase difference between the time history is one clue that shows the blades are "not" lead-lagging in a predominately collective manner.

Figure 20 shows the time history, FFT and Moving Block plots for the cosine lag and sine lag components obtained from MCT for Run 9, Point 5. From the cosine component, a sharp peak exists at the regressing lag frequency, 1.38 Hz. The damping estimated from the Moving Block is 2.65%. The result for the sine component is similar to that of the cosine component because they "combine" together to cause regressing and progressing lag modes. The difference is, for a soft-inplane rotor at the operating rotor speed,

the cosine lag time history always leads the sine lag time history by 90 degrees, for both regressing and progressing lag modes [9,10,11].

When the swashplate excitation in the fixed frame is at the regressing lag frequency, then the rotating frame lag motion is dominated by the regressing lag motion, and there is very little collective lag motion, and almost no progressing lag motion.

A comparison of the decay rate for the regressing lag measured in the rotating frame (Fig. 18) and in the fixed frame (Fig. 20) shows they are nearly identical.

1L	$\zeta$	$\omega$ (Hz)	$\zeta\omega$
Rot. frame	.0099	3.84	.038
Fixed frame	.0265	1.38	.037

Even though the collective lag motion in Run 9, Point 5 is minuscule, it can still be extracted using MCT. Figure 21 shows the collective lag component time history, FFT and Moving Block results for the same hover case. The peak at 2.8 Hz is the collective lag mode. A comparison of the FFT amplitude of Fig. 21 to that in Fig. 20, shows the collective lag component is much weaker (160 in-lbs vs. 5,000 in-lbs). Notice that the collective frequency is less than the rotating frame lag frequency (3.8 Hz) because collective lag is coupled with the shaft and transmission flexibility. The frequency spectrum of collective

lag from the Chirp test (Fig. 7) also confirms the collective mode is around 2.8 Hz. The damping for the collective mode is 1.21%. This gives a decay rate of  $(\zeta\omega)_{col. lag} = 0.0121 \times 2.8 \text{ Hz} = 0.034 \text{ cycle/sec}$ . Alternatively, CIPHER analysis has also been used to obtain modal dampings by doing a modal curve fit of Figs. 6 and 7.

For an isolated rotor, with minimal coupling between the rotor and hub motions, the decay rates  $(\zeta\omega)$  are "similar" between that measured in the rotating frame for an isolated blade, and that measured in the fixed frame for the "rotor" collective and regressing modes. But, the damping ratios  $(\zeta)$  are different.

### Progressing Lag Mode

The progressing lag mode decay rate is more difficult to excite sufficiently to give a strong signal. Figure 22 shows the rotating frame lead-lag time history, the dynamic actuator time history, the FFT and Moving Block for Run 13, Point 12. The rotor was shaken at 9 Hz, the progressing lag mode frequency in the fixed frame. Using the time history from 0.9 to 2.5 seconds, the frequency measured in the rotating frame from FB1EB12 gauge is 3.75 Hz, and the damping ratio  $(\zeta)$  is 4.7%.

Figure 23 presents the cosine lag component time history, FFT, and Moving Block for Run 13, point 12 obtained from a MCT. Using the time history from 0.9 to 2.5 seconds, the frequency measured in the fixed frame is 8.98 Hz, and the damping ratio  $(\zeta)$  is between 1.5% to 2.1%.

A comparison of the decay rate for the progressing lag measured in the rotating frame (Fig. 22) and in the fixed frame (Fig. 23) shows they are similar, as expected.

1L	$\zeta$	$\omega$ (Hz)	$\zeta\omega$
Rot. frame	.047	3.75	.18
Fixed frame	.015 to .021	8.98	.14 to .19

This shows the progressing lag mode decay rate is significantly higher than the regressing lag mode decay rate. Reference [11] has also shown that for an isolated rotor the progressing lag mode decay rate  $(\zeta\omega)$  is usually the highest among all the rotor lag modes; this is due to dynamic inflow.

Reference [11] shows when hub motion is included, then collective lag decay rate becomes slightly higher than the progressing lag mode, because the progressing whirl becomes slightly coupled with the hub motion. But, the low frequency regressing lag mode is always the least stable mode.

### Stability and Frequency of the Second Lag Mode

Figure 24 shows the rotating frame time history, FFT and Moving Block from FB1EB12 for a hovering case with 2 degrees of collective at 3/4 span (Run 9, Point 28). The rotor was shaken at the 2nd lag mode's regressing lag frequency (19.7 Hz). The FFT shows the rotating frame 2L frequency is 25.3 Hz. The critical damping in the rotating frame was determined to be between 3.2% and 1.13%.

Figure 25 shows the time history, FFT and Moving Block in the fixed frame, for the collective component of the 2nd lag mode. The spikes in time history at between 1.5 and 2 seconds are due to a jolt in the dynamic actuators. But, the FFT and Moving Block results only include the time history between the excitation shutoff and the jolt. The measured 2nd lag collective mode frequency is 25.2 Hz. This is very close to the rotating frame 2L frequency of 25.3 Hz. This implies the 2L mode is not coupled with the RTA stand or transmission.

Figure 26 shows the time history, FFT and Moving Block in the fixed frame, for the cosine component of the 2nd lag mode. The frequency is at 19.97 Hz. The FFT looks very clean, and the two peaks are very sharp. The 2Lprog mode is not visible in the FFT because the rotor was shaken at 19.7 Hz, hence the 2Lprog mode was not excited. Moving Block analysis shows the damping in the fixed frame is 4.16%.

A comparison of the decay rate for the 2nd lag modes in the rotating frame and fixed frame is shown below:

2L	$\zeta$	$\omega$ (Hz)	$\zeta\omega$
Rot. frame	.011 to .032	25.3	.29 to .81
Reg. lag	.0416	19.97	.83
Col. lag	.0289	25.2	.73

### Inplane Motion for the Lag Modes

Figure 27 shows a very interesting plot. It is generated from the transient decay during a hover stability test (Run 13, Point 7). The cosine lag time history,  $\zeta_{1C}(t)$  is plotted against the sine lag time history,  $\zeta_{1S}(t)$ . This trace represents the location of the rotor center-of-mass as seen from above the rotor. Approximately twelve small loops are formed, these represent the 1P oscillation. They are labeled in the figure. At the same time, the center-of-mass is also tracing out large circular loops. About three and 3/4 revolutions of the large loops have been completed. These represent the "forward" whirling nature of the regressing lag mode: the center-of-mass rotates in the same direction as the rotor's rotation. If the number of cycles (3-3/4) is divided by the trace duration (2.8 sec), then it yields the regressing lag frequency (1.3 Hz). Since the diameter of the large circular pattern diminishes with time, the regressing lag mode is stable.

Figure 28 shows the trace for the same Run 13, Point 7, plotted for the entire transient decay, from 0 to 8 seconds. It shows the circular pattern is shrinking with respect to time. In Run 13, Point 7 the rotor was shaken using only one of the three dynamic actuators (only D3 was used), this gives a combination of collective and cyclic inputs. Even though it was not a nutation excitation, the resulting trace shows the inplane motion is still dominated by the large circular pattern of the regressing lag mode.

Figure 29 shows the time trace for Run 9, Point 5, from  $t = 2.95$  second to  $t = 4.0$  second. For this test point, the swashplate was shaken in a nutation manner. The resulting trace is similar to that from shaking with a single actuator. The trace in Fig. 29 is dominated by the regressing lag mode and 1P lag motion. In Fig. 29, about 1-1/4 revolution of the big circle was completed during the 1.05 second time span, this gives a frequency of 1.2 Hz. Also, about 5.5 cycles of small circles were completed in 1.05 second, this gives a frequency of 5.24 Hz.

Figure 30 shows the time history for the rotor when it was shaken at 9 Hz in the nonrotating frame with actuator D3 only (Run 13, Point 12). The actuator was cut off at  $t = 0.9$  second. The

time history shown here is from 0.9 to 2.5 second. The  $\zeta_{1C}(t)$  vs.  $\zeta_{1S}(t)$  trace shows the rotor center-of-mass whirls forward at a rate around 8.9 Hz (14.5 cycles were counted in 1.6 seconds). This decay is dominated by progressing lag only. Notice the center-of-mass whirls forward, in the same direction as the rotor's rotation, and it decays very rapidly.

Figure 31 shows the trace from 2.9 to 4 seconds for the same case (Run 13, Point 12). As expected, this trace is dominated by 1P because the progressing lag motion has died out. 5.6 cycles were counted during this 1.1 second period, this gives a frequency of 5.1 Hz. Notice the amplitude is not decaying, and it is around +/- 4,000 in-lbs.

These  $\zeta_{1C}(t)$  vs.  $\zeta_{1S}(t)$  traces offer valuable physical insights into rotor stability analysis. They provide the following informations:

- (1) The number of cycles during a specified period gives information about modal frequency.
- (2) The number of types of loop tells about the number of modes in existence.
- (3) The radius of the loops tells the amplitude of mass wobble.
- (4) The rate of growth or shrinkage of the radius describes the stability of the system.
- (5) The direction of the whirl provides physical understanding of rotor motion. For a soft-inplane rotor, at the nominal rpm, both regressing and progressing lag modes whirl in a forward direction.
- (6) The roundness of the regressing lag loops determine the level of rotor/body coupling. A round circle means the regressing lag is not coupled to the body (assuming the body does not have identical pitch and roll mode natural frequencies).

### CONCLUSIONS

1. The Sikorsky S-76 BMR is stable at all the conditions tested.
2. Lag mode stability depends on the displacement of the snubber/damper. The nonlinear stiffness and damping

characteristics must be accounted for in order to predict stability accurately.

3. As 1/rev lag motion increases, the BMR with elastic snubber/damper as shown has increasing stability (this is beneficial).
4. Cyclic sweep, N-per-rev frequency crossing, and Chirp excitation are useful for obtaining rotor frequencies experimentally.
5. With all five blades instrumented, then the progressing, 2nd progressing, and 2nd regressing lag mode frequencies can be determined readily.
6. It is not necessary to nutate the swashplate to excite the regressing lag mode. A proper selection of the fixed frame excitation frequency determines the type of rotor mode that will be excited.
7. If the rotor is shaken at the fixed frame regressing lag frequency, then the lag damping measured in the rotating frame from a single blade is very close to the true regressing lag mode damping for the whole rotor. This was shown experimentally by comparing the decay rate from the single blade and the decay rate from the cosine, or sine lag component, in the fixed frame.
8. Instrumenting all rotor blades with flap and lag strain gages can provide physical insight on the rotor motion. It also permits getting the collective mode frequency and damping.
9. Even for an isolated rotor, the collective lag frequency is very different from the rotating frame lag frequency because it is coupled with the transmission.
10. This experiment has shown that for a soft-inplane rotor, the cosine lag leads the sine lag component by  $90^\circ$  for both regressing and progressing lag modes. Their frequency spectrums are almost identical.
11. Experimental results and analyses demonstrate that, even for an isolated rotor, the decay rate for the collective, regressing, and progressing lag modes are not identical. The decay rate for the progressing lag is usually higher than the other lag modes. This

effect can be captured analytically when dynamic inflow is used.

## REFERENCES

- [1] Norman, T. R., Cooper, C. R., Fredrickson, C. A., and Herter, J. R., "Full-scale Wind Tunnel Evaluation of the Sikorsky Five-bladed Bearingless Main Rotor," presented at the 49th Annual Forum of the American Helicopter Society, St Louis, Missouri, May 19-21, 1993.
- [2] Kottapalli, S., Swanson, S., LeMasurier, P., Wang, J. M., "Full-scale Higher Harmonic Control Research to Reduce Hub Loads and Noise," presented at the 49th Annual Forum of the American Helicopter Society, St Louis, Missouri, May 19-21, 1993.
- [3] Sopher, R., and Cassarino, S. J., "Effects of Analytical Modeling Assumptions on the Predicted Stability of a Model Hingeless Rotor," presented at the 41th Annual Forum of the American Helicopter Society, Ft. Worth, TX, May 1985.
- [4] Sopher, R., and Chen S. Y., "Application of Component Mode Synthesis to Modeling the Dynamic Response of Bearingless Main Rotors," presented at the 48th Annual Forum of the American Helicopter Society, Washington D.C., June 1992.
- [5] Sopher, R., and Hallock, D.W., "Time-History Analysis for Rotorcraft Dynamics Based on a Component Approach," *Journal of the American Helicopter Society*, Vol. 31, (1), January 1986, pp 43-51.
- [6] Torok, M. S., and Goodman, R. K., "Analysis of Rotor Blade Dynamics Using Experimental UH-60A Airloads Obtained at the DNW," presented at the 47th Annual Forum of the American Helicopter Society, Phoenix AZ, May 1991.
- [7] Wang, J. M., Chopra, I., Green, M., Samak, D.K. and Graham, T., "Theoretical and Experimental Investigation of the Aeroelastic Stability of an Advanced Bearingless Rotor in Hover and Forward Flight," presented at the National Specialists Meeting on Rotorcraft Dynamics, Arlington, TX, Nov. 1989.

- [8] Wang, J. M., and Chopra, I., "Bearingless Rotor Aeromechanical Stability Measurement and Correlation Using Nonlinear Aerodynamics," presented at the 16th European Rotorcraft Forum, Glasgow, Scotland, Sept. 1990.
- [9] Wang, J. M., and Chopra, I., "Dynamics of Helicopters in Ground Resonance with and Without Blade Dissimilarities," presented at the AIAA Dynamics Specialists Conference, Dallas, TX, April 16-17, 1992.
- [10] Wang, J. M., and Chopra, I., "Dynamics of Helicopters with Dissimilar Blades," presented at the 47th Annual Forum of the American Helicopter Society, Phoenix AZ, May 1991.
- [11] Wang, J. M., "Aeromechanical Stability of Helicopters with Dissimilar Blades," PhD dissertation, Aerospace Department, University of Maryland, College Park, MD, May, 1992.
- [12] Tischler, M. B., and Cauffman, M. G., "Frequency-Response Method for Rotorcraft System Identification: Flight Applications to BO 105 Coupled Rotor/Fuselage Dynamics," *Journal of the American Helicopter Society*, Vol. 37, (3), July 1992, pp. 3 - 17.
- [13] Pitt, D. M., and Peters, D. A., "Theoretical Prediction of Dynamic Inflow Derivatives," *Vertica*, Vol. 5, (1), 1981, pp. 21 - 34.

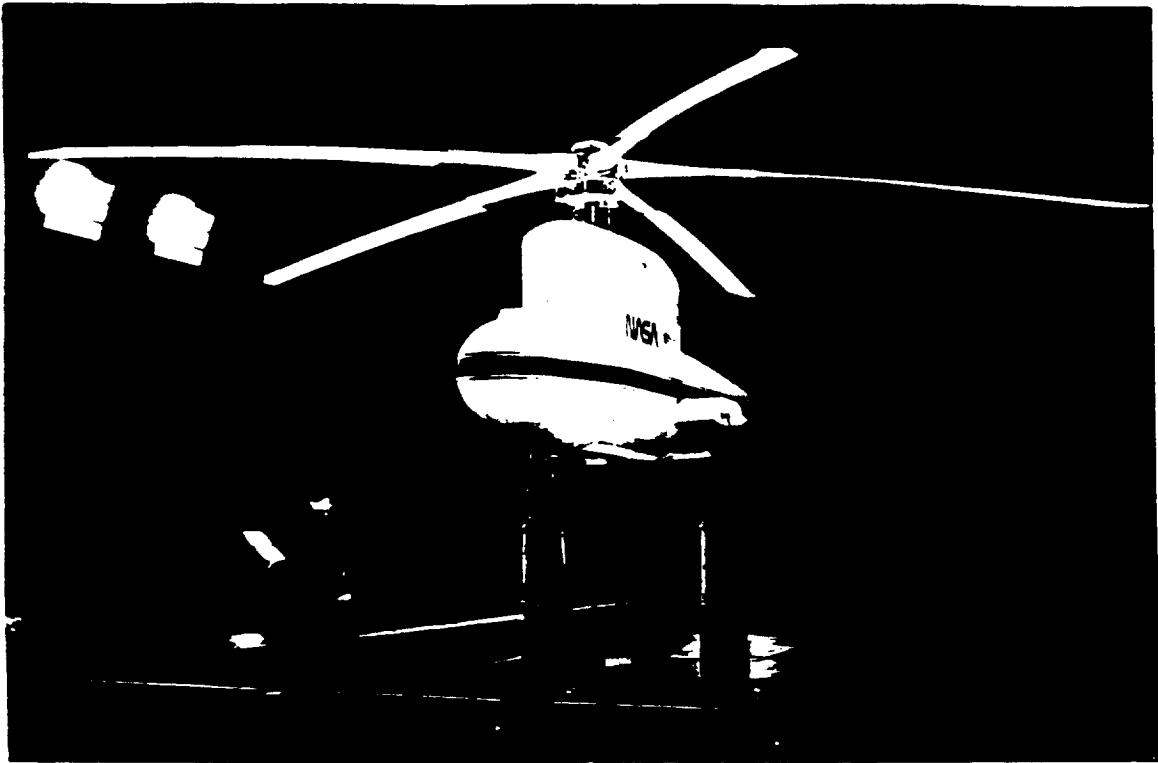


Fig. 1 Sikorsky proof-of-concept 5-bladed bearingless main rotor inside NASA Ames 40'x80' Wind Tunnel.

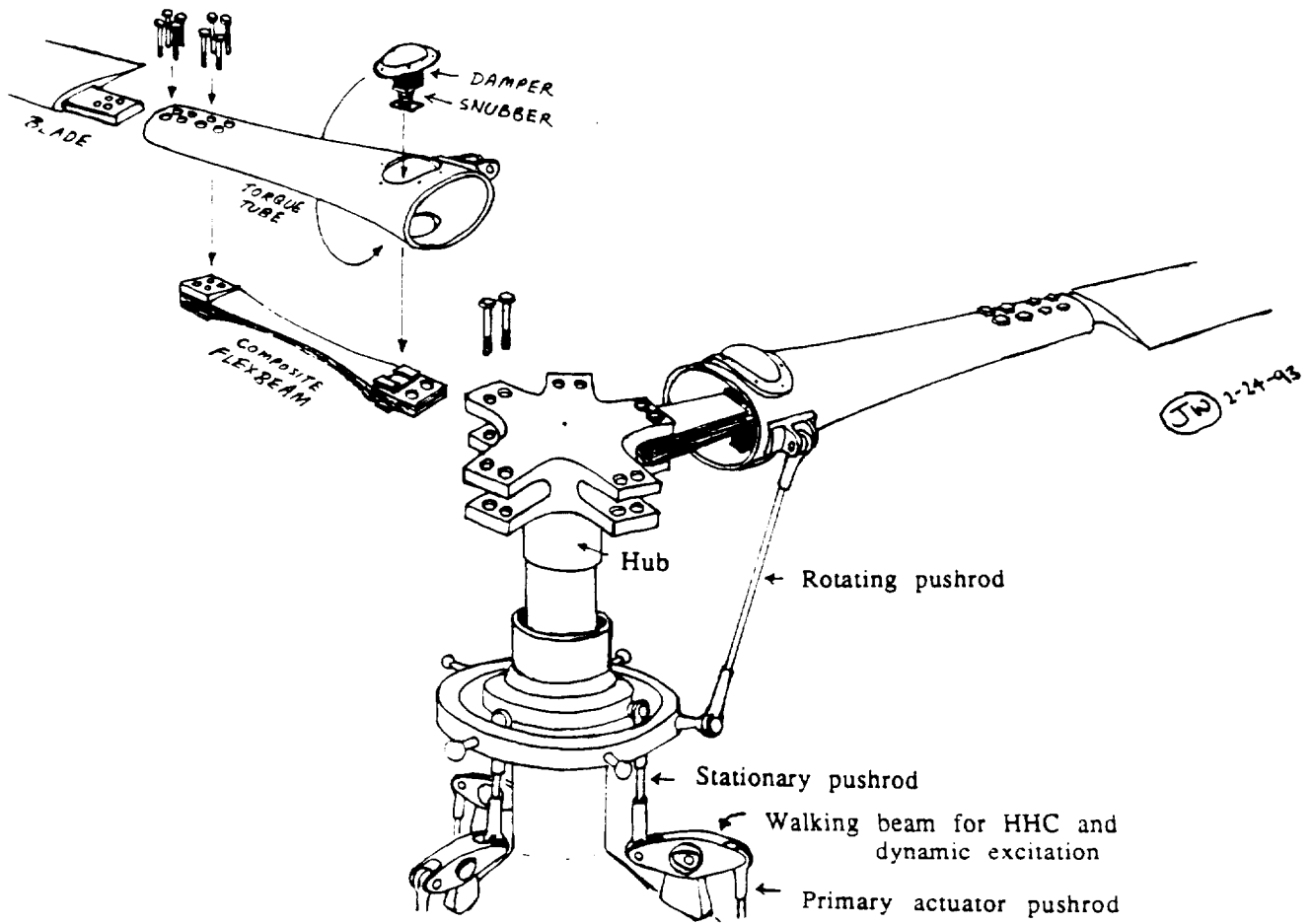


Fig. 2 Sikorsky S-76 5-bladed bearingless main rotor design.

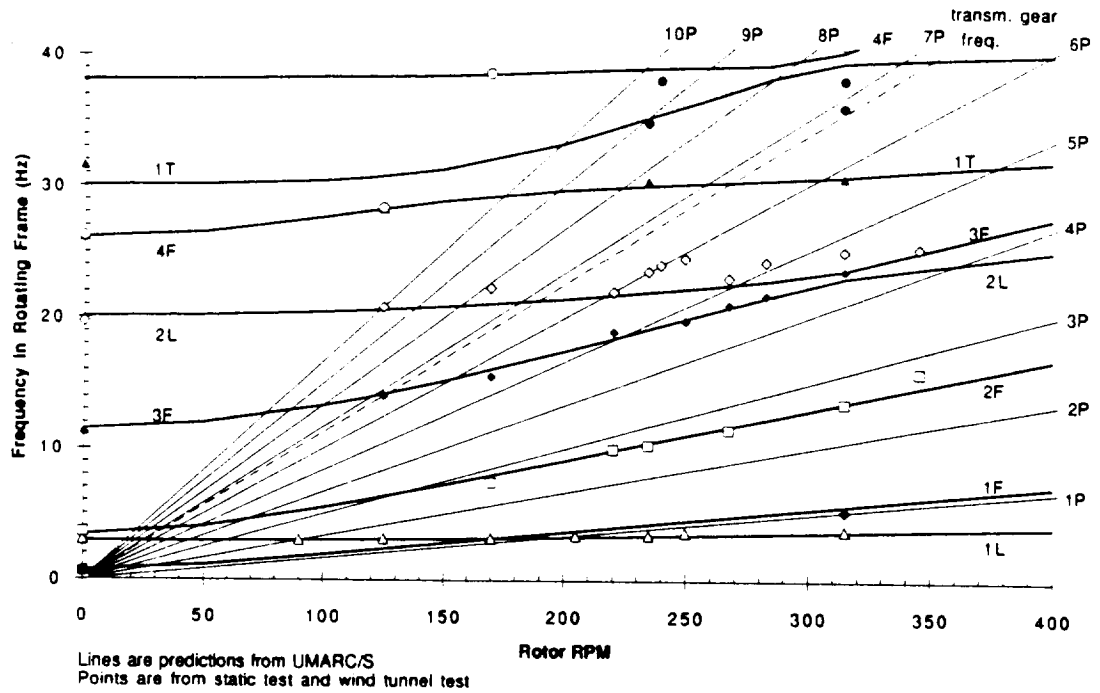


Fig. 3 Measured and calculated Southwell frequency diagram.

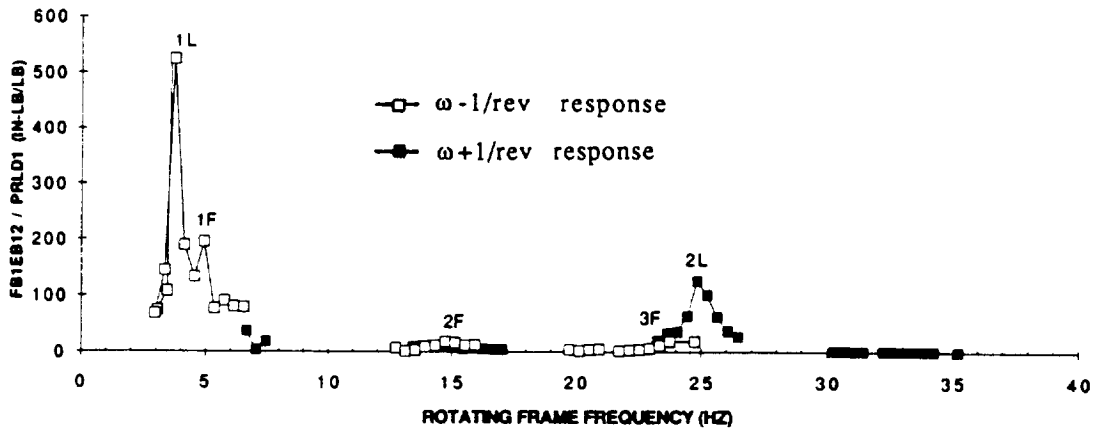


Fig. 4 Blade edgewise moment response measured from a swashplate cyclic frequency sweep. The edgewise response (EB12) is normalized by the rotating pushrod load (PRLD1).

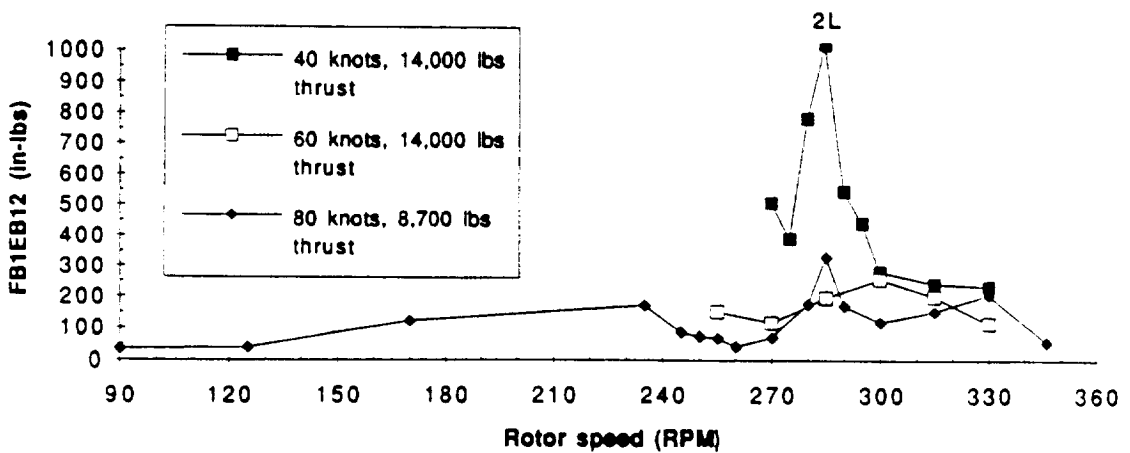


Fig. 5 Blade edgewise 5P moment response measured from rotorspeed sweeps.

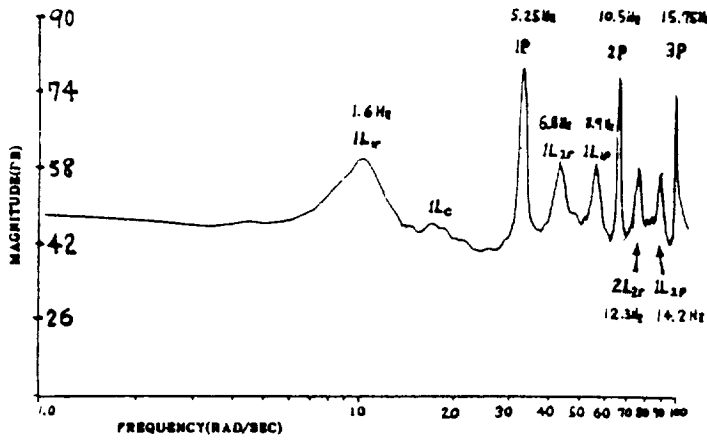


Fig. 6 Bode plot generated from the cosine lag component,  $\zeta_{1C}(t)$ . A 0.8 to 12 Hz Chirp was used.

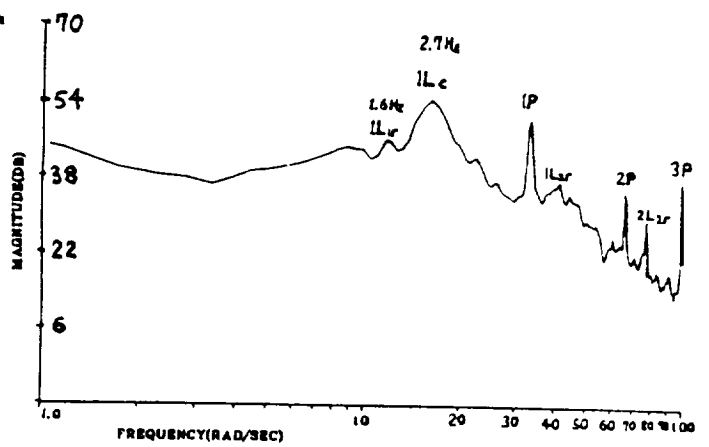


Fig. 7 Bode plot generated from the collective lag component,  $\zeta_o(t)$ . A 0.8 to 12 Hz Chirp was used.

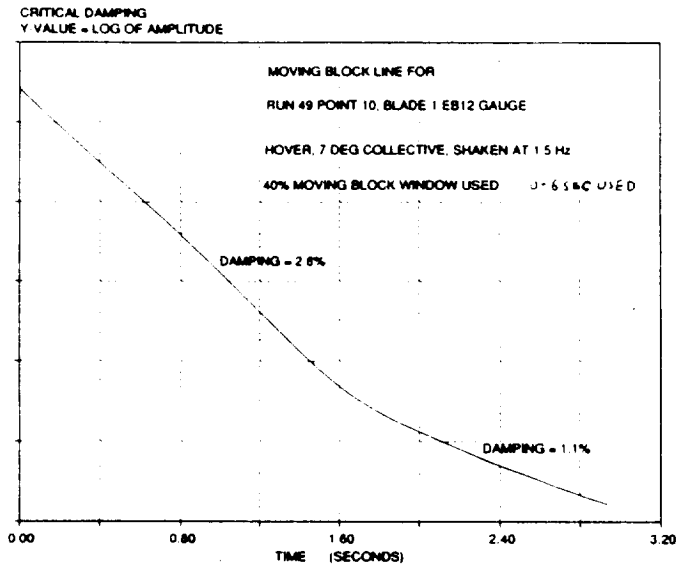


Fig. 8a Example of the nonlinear damping phenomenon of the snubber damper.

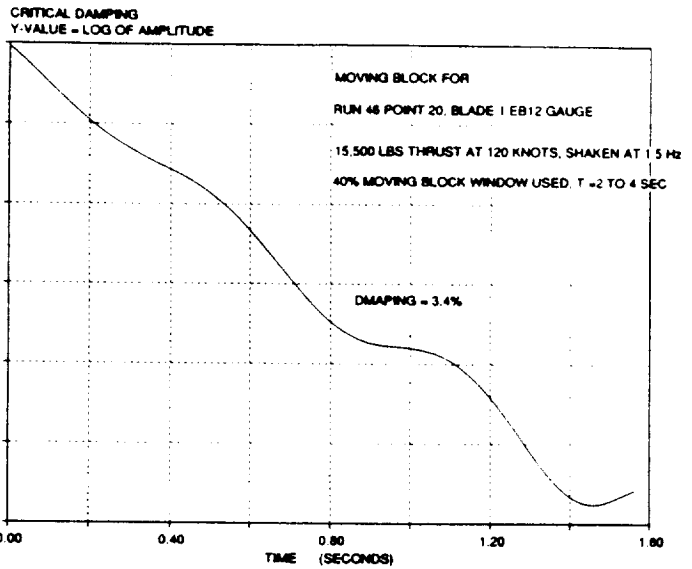


Fig. 8b Example of ripples seen in the Moving Block line for forward flight data.

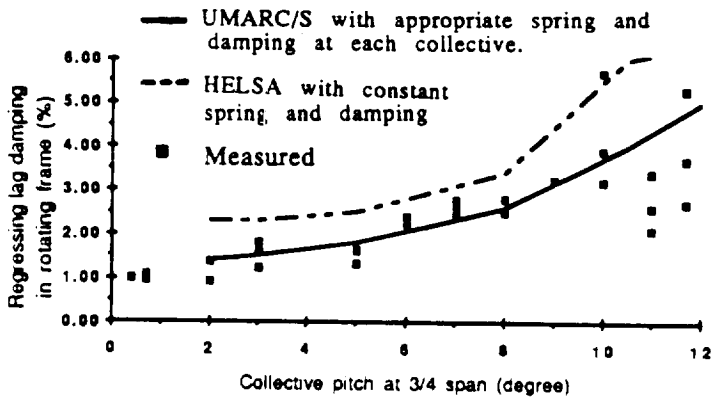


Fig. 9 Measured and predicted hover stability.

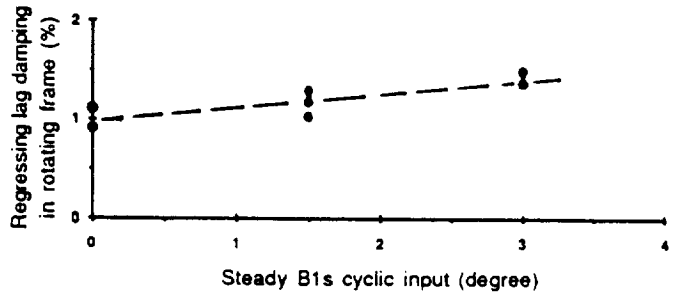


Fig. 10 Effect of longitudinal cyclic on lag stability. Positive B<sub>1s</sub> = forward cyclic.

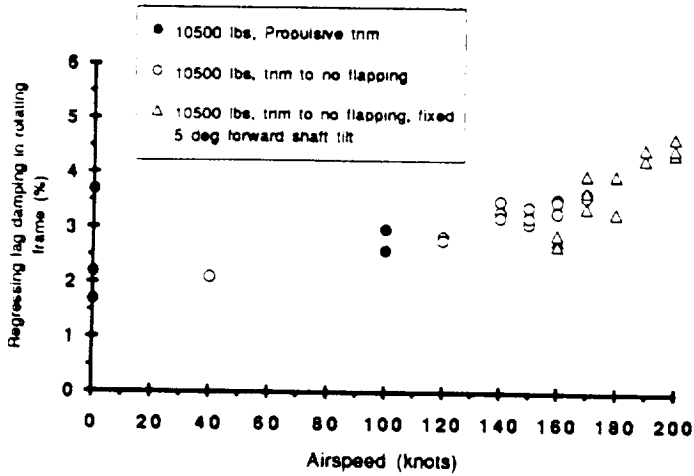


Fig. 11 Measured lag mode damping ratio vs. tunnel speed for 10,500 lbs thrust.

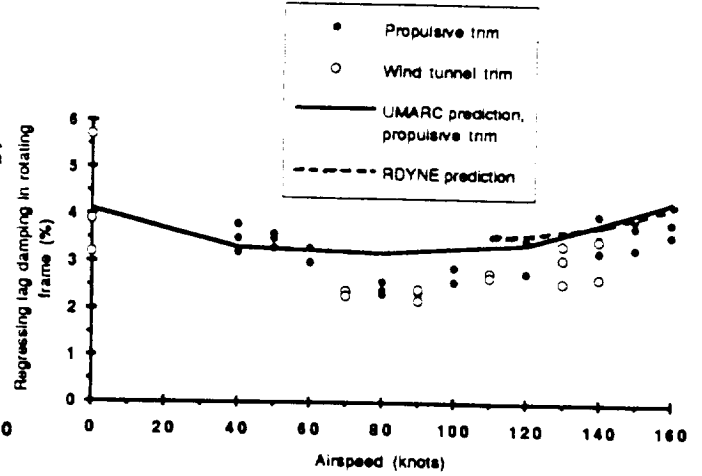


Fig. 12 Measured and predicted lag mode damping ratio vs. tunnel speed for 14,000 lbs thrust.

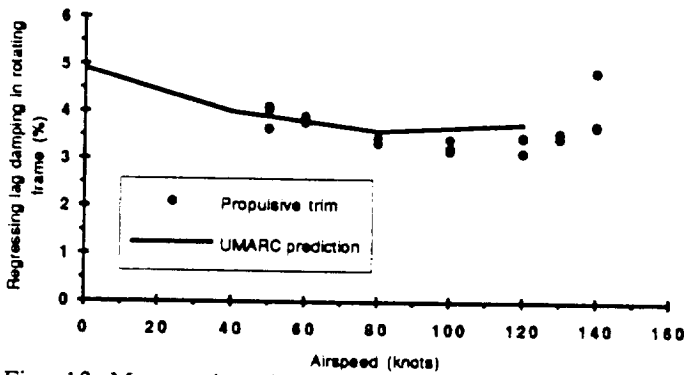


Fig. 13 Measured and predicted lag mode damping ratio vs. tunnel speed for 16,000 lbs thrust.

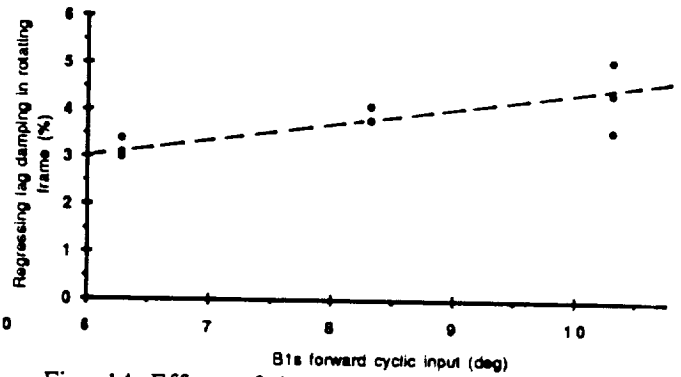


Fig. 14 Effect of longitudinal cyclic on lag stability at 120 knots. Positive  $B_{1S}$  = forward cyclic.

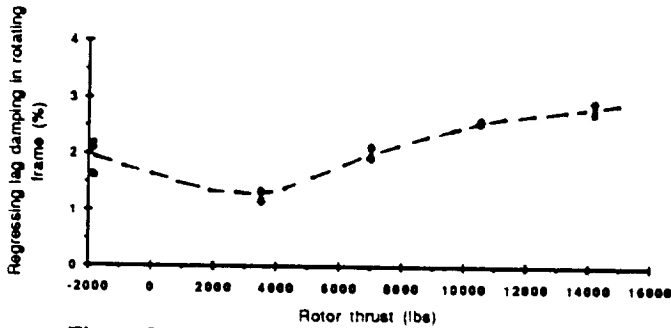


Fig. 15 Effect of rotor thrust on lag stability at 80 knots. Propulsive trim was used.

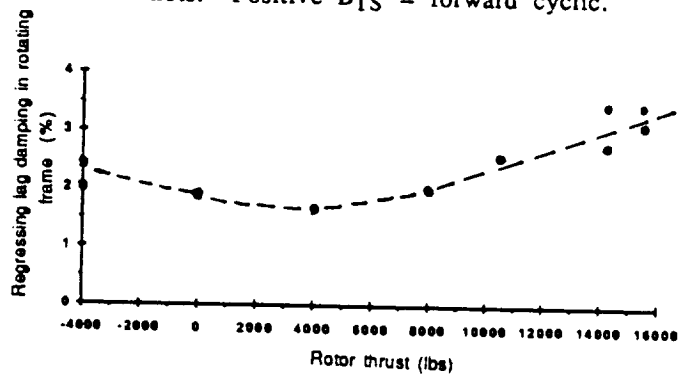


Fig. 16 Effect of rotor thrust on lag stability at 120 knots. Propulsive trim was used.

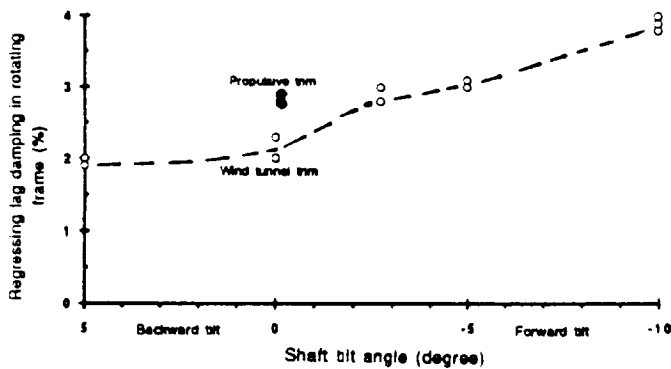


Fig. 17 Effect of shaft angle on lag stability at 80 knots, and steady 14,000 lbs thrust.

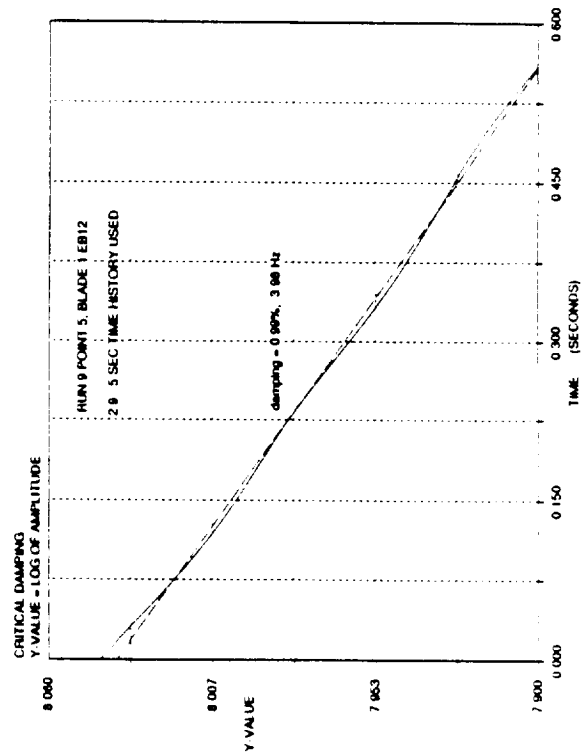
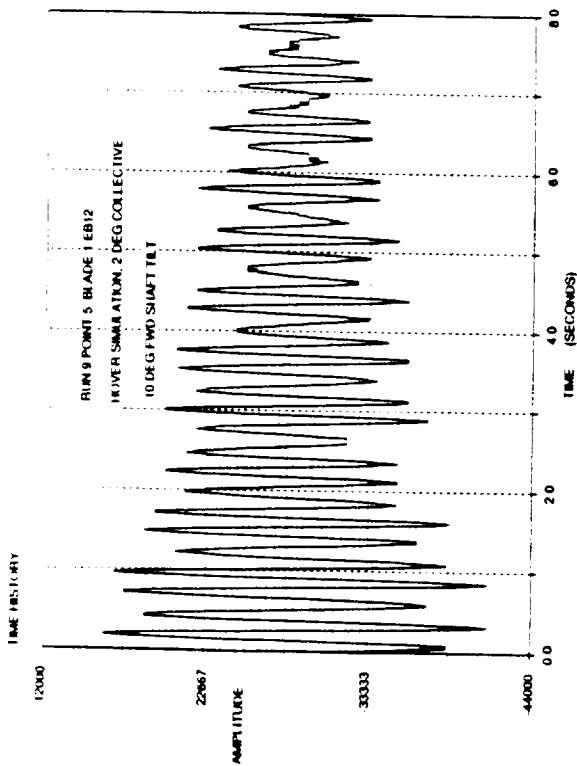
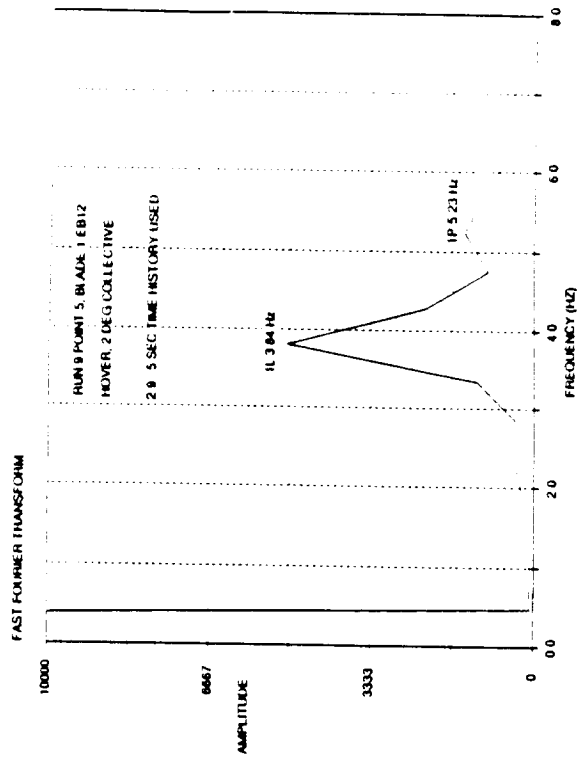


Fig. 18 Time history, FFT and Moving Block results from blade 1 edgewise bending strain gauge (FBIEB12) in the rotating frame. Shaken at the fixed frame regressing lag frequency, 1.5 Hz. (Run 9, Point 5)

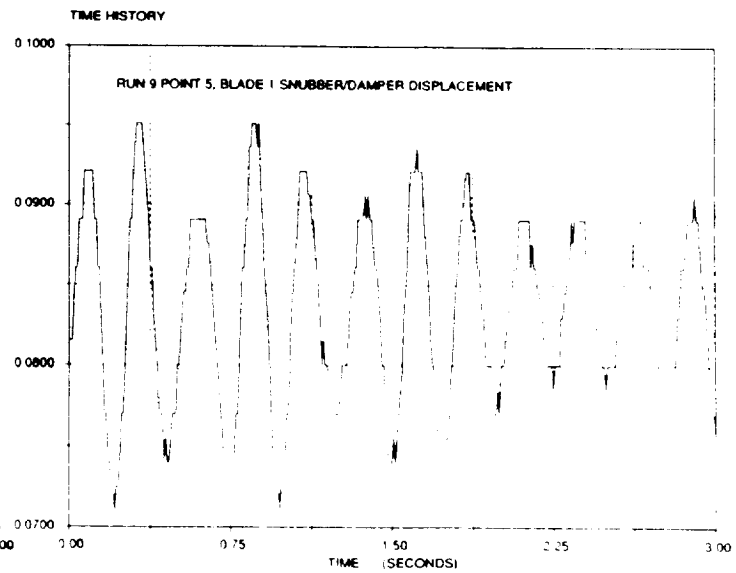
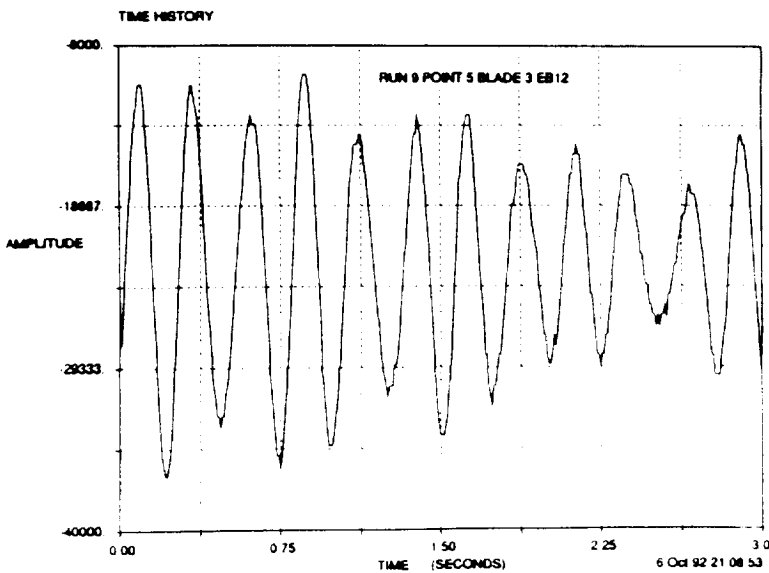
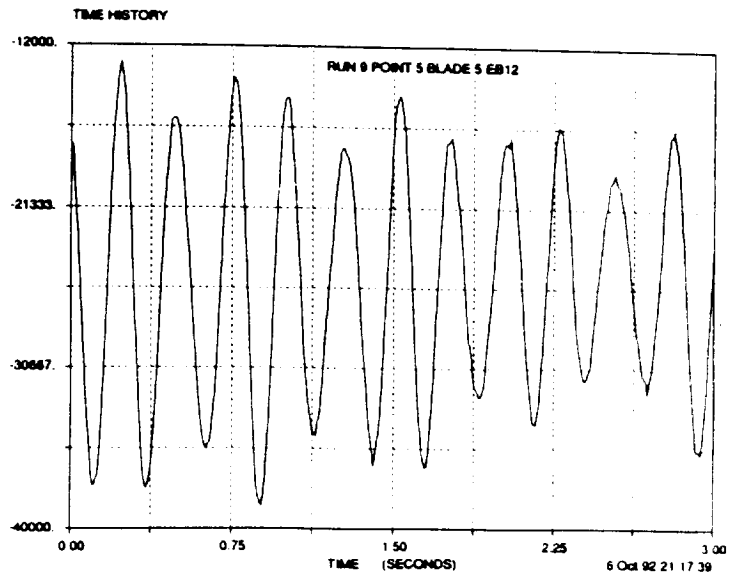
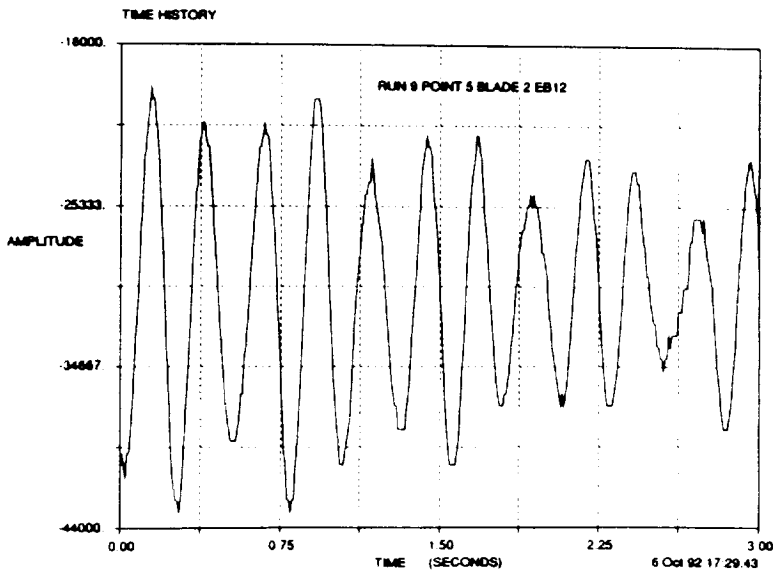
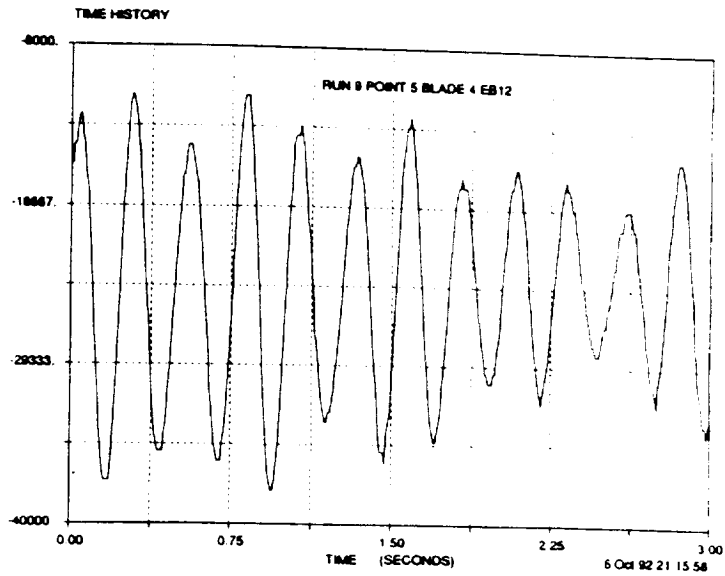
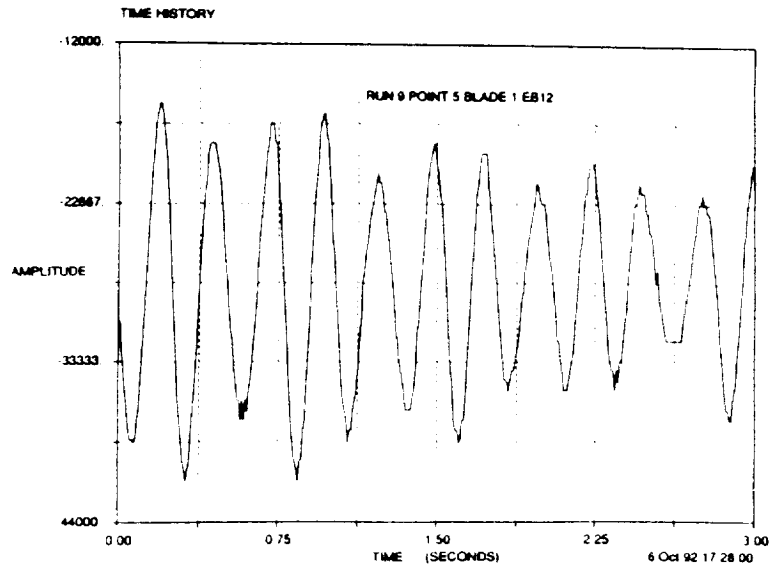


Fig. 19 Measured time history in the rotating frame for all five blades, and the snubber/damper displacement from blade 1. (Run 9, Point 5)

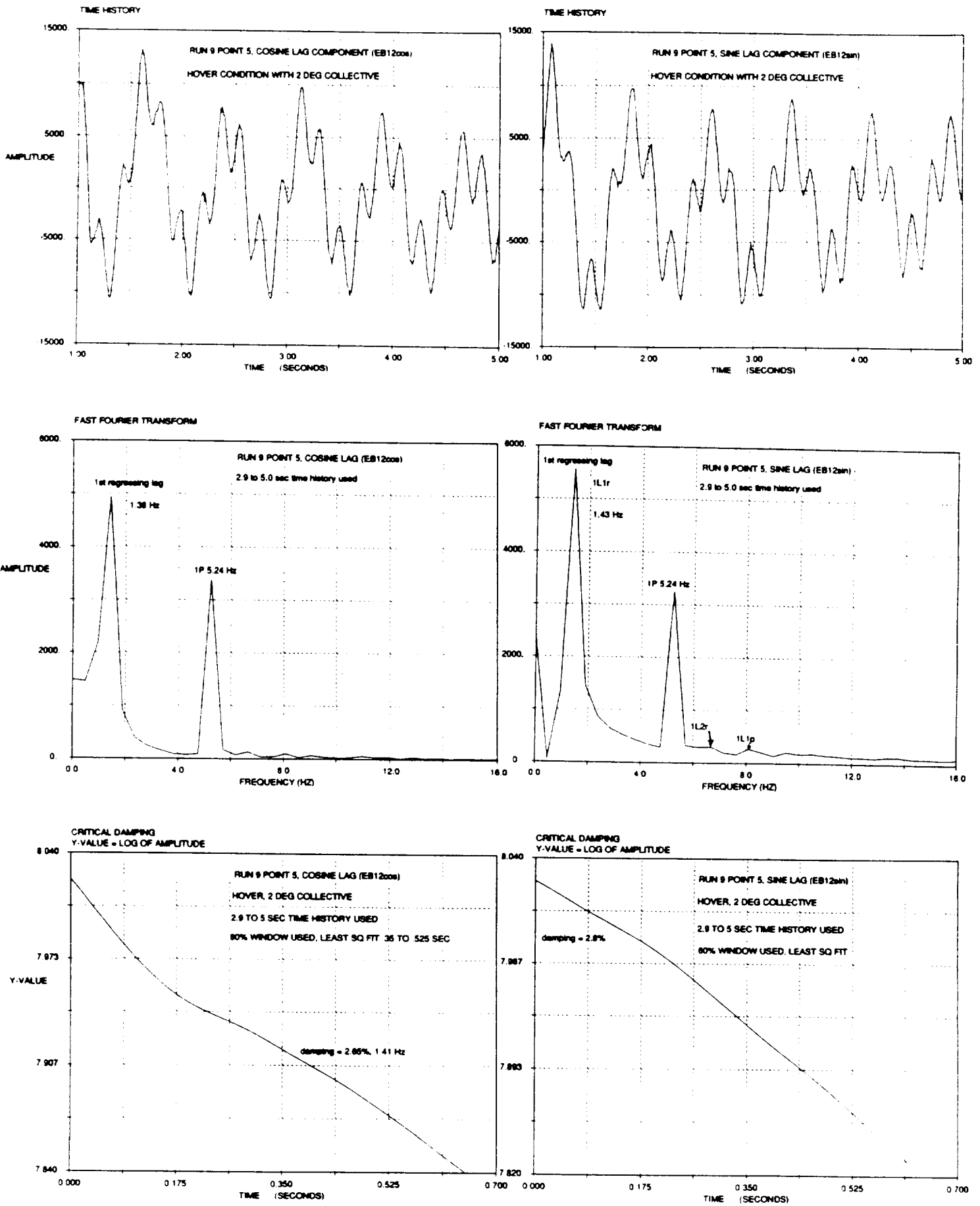


Fig. 20 Time history, FFT and Moving Block for the cosine and sine lag components. (Run 9, Point 5)

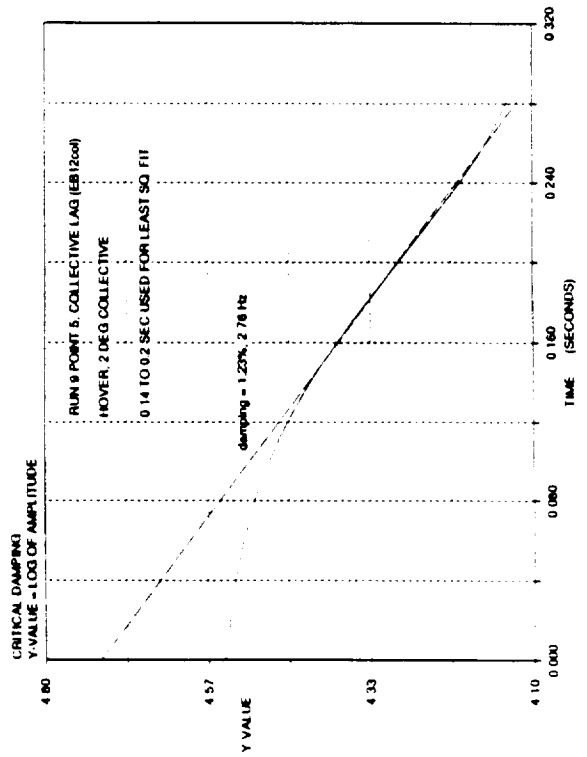
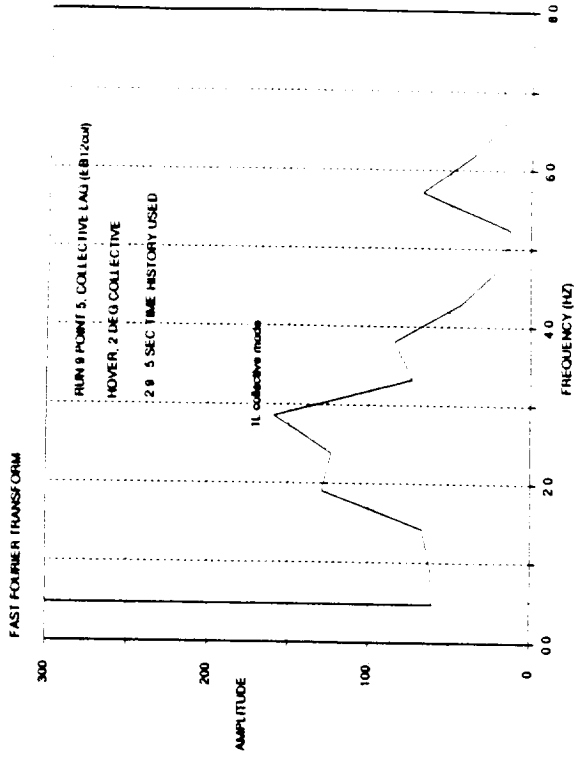
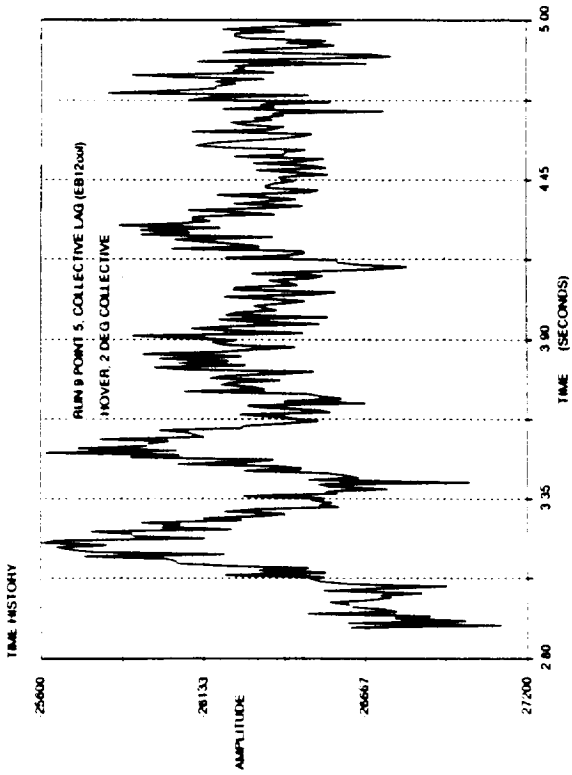


Fig. 21 Time history, FFT and Moving Block results from collective lag component in the fixed frame. (Run 9, Point 5)

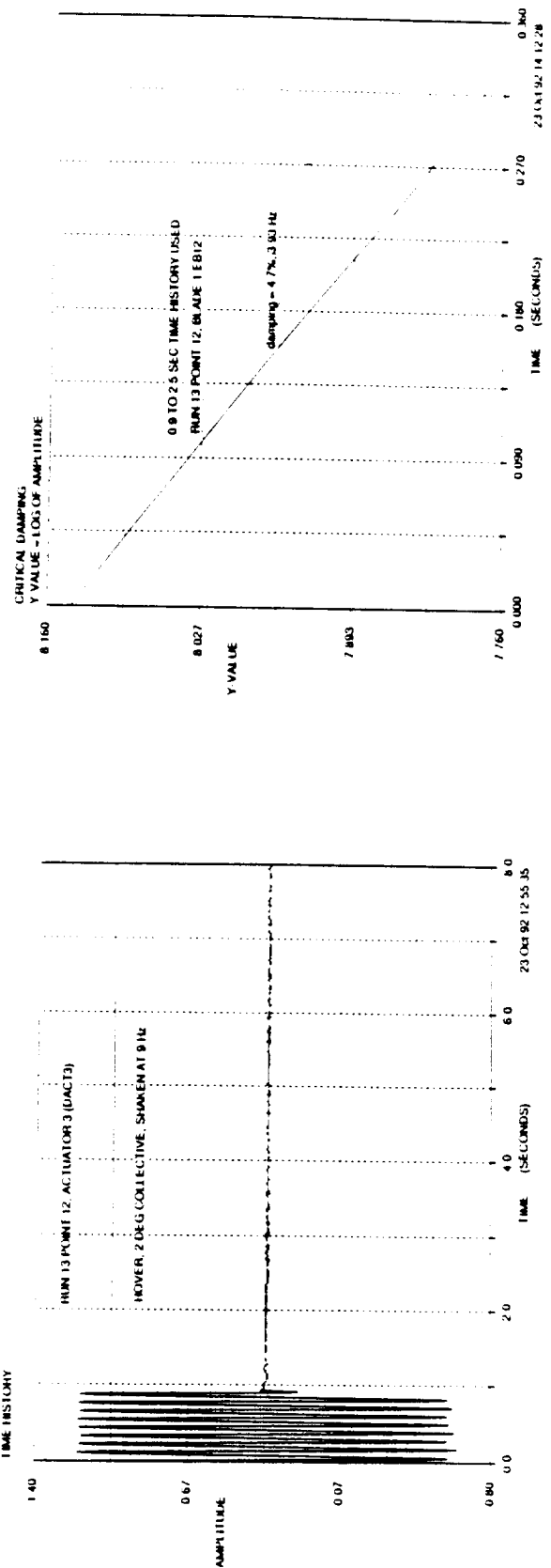
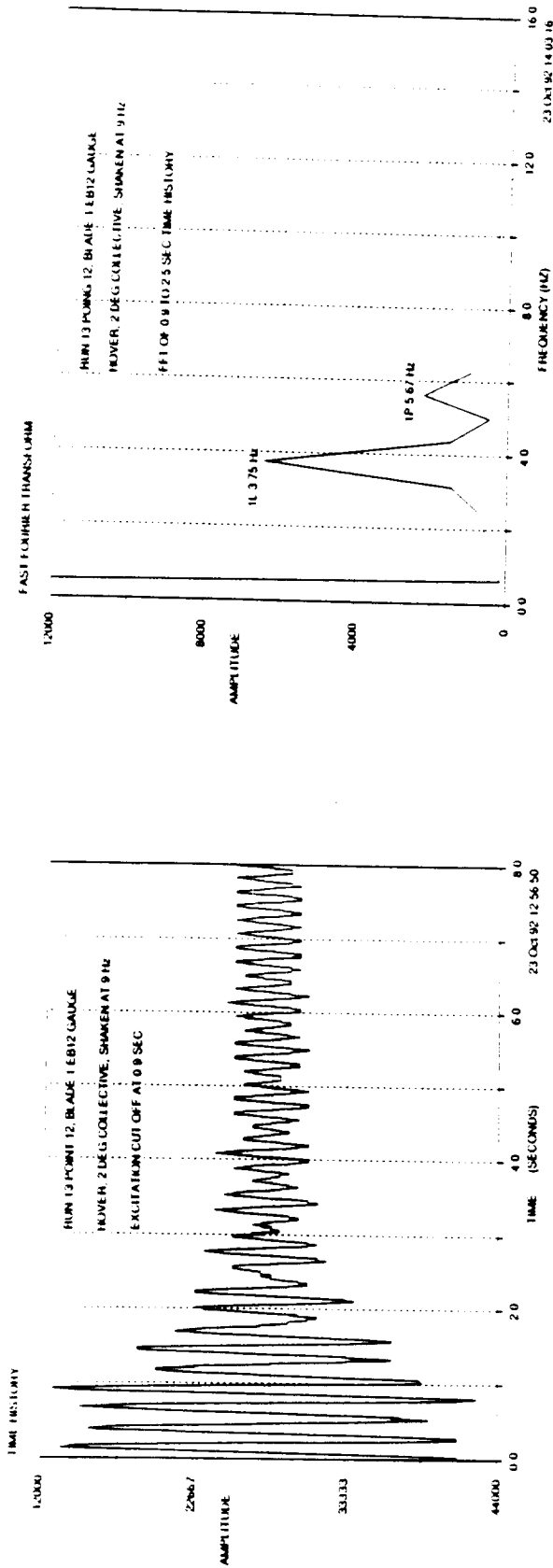


Fig. 22 Time history, FFT and Moving Block results from blade 1 edgewise bending strain gauge (FB1EB12) in the rotating frame. Shaken at the fixed frame progressing lag frequency, 9 Hz. (Run 13, Point 12)

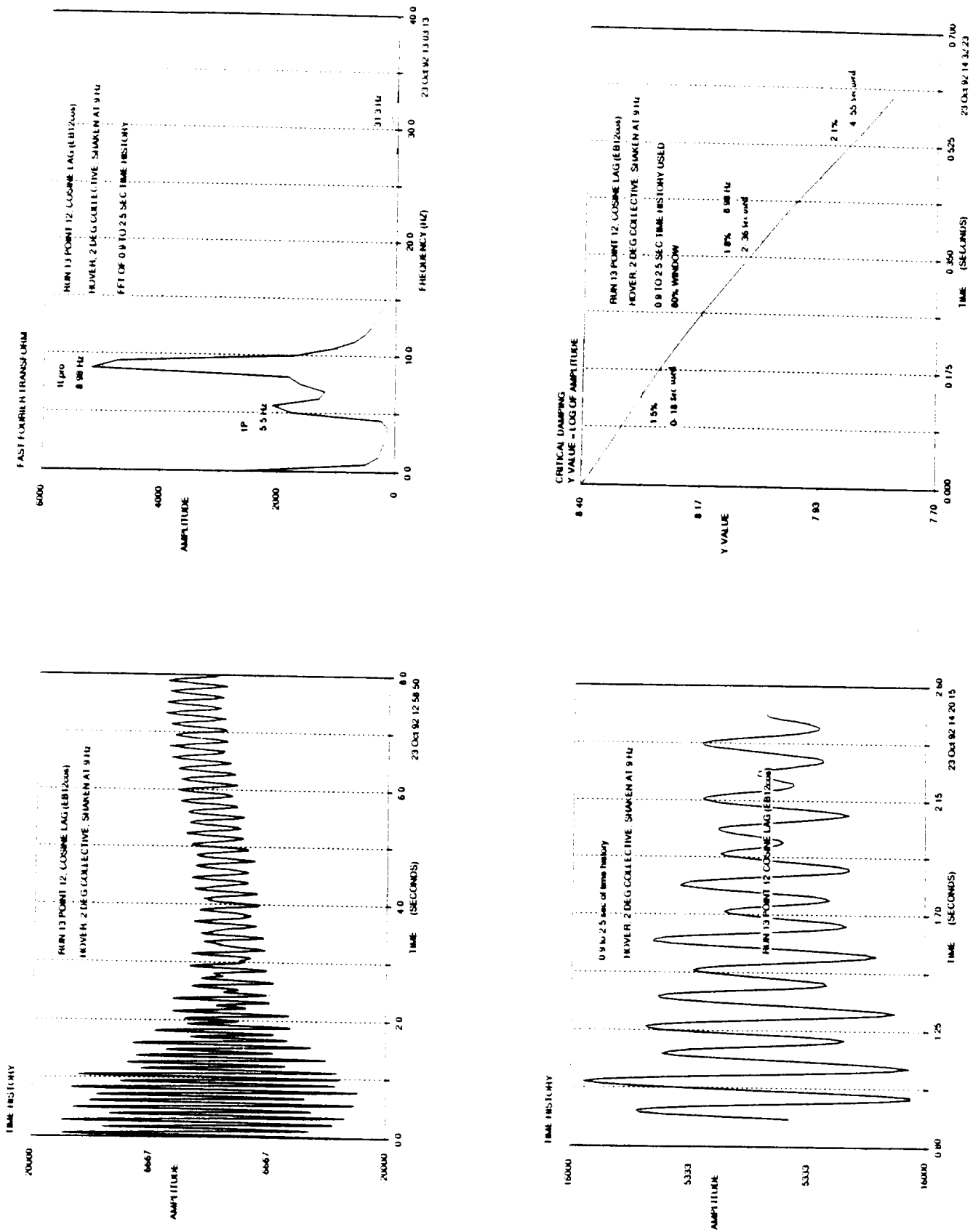


Fig. 23 Time history, FFT and Moving Block results for the cosine lag component in the fixed frame. Shaken at the fixed frame progressing lag frequency, 9 Hz. (Run 13, Point 12)

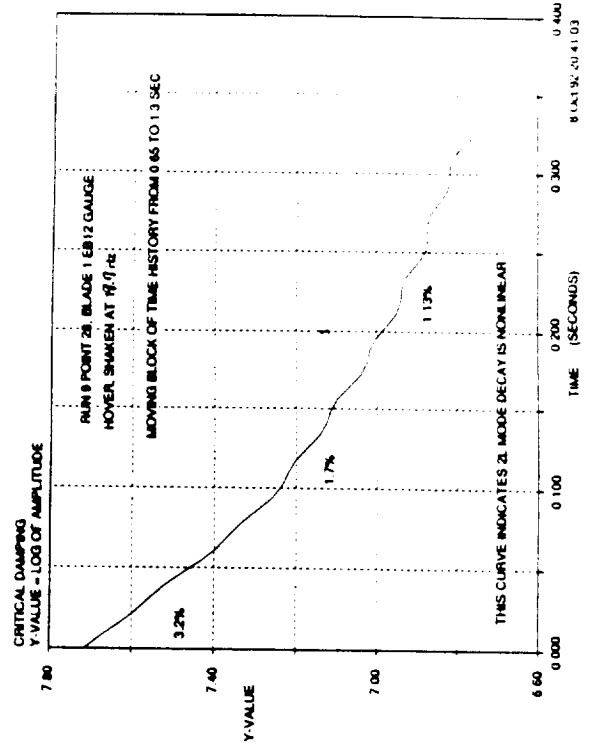
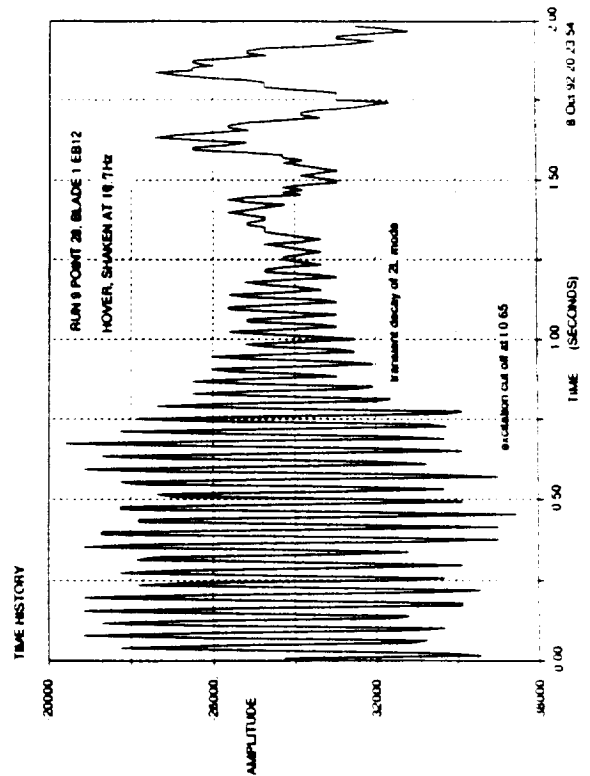
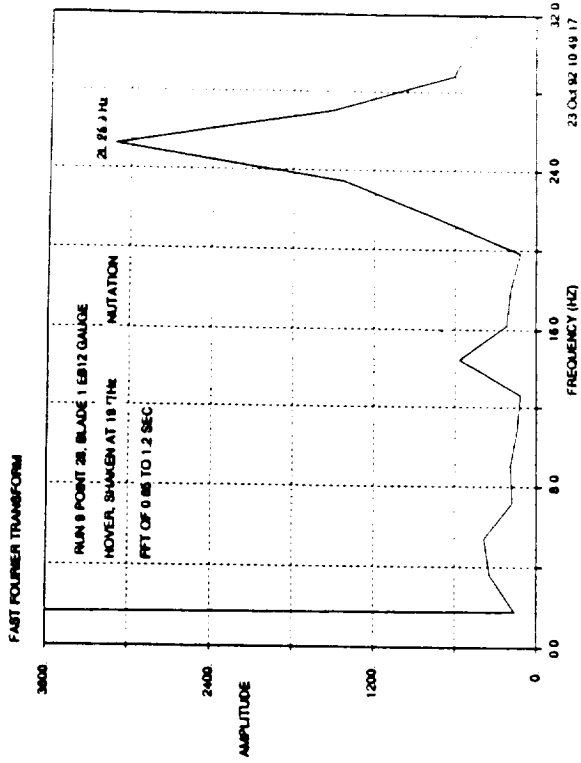
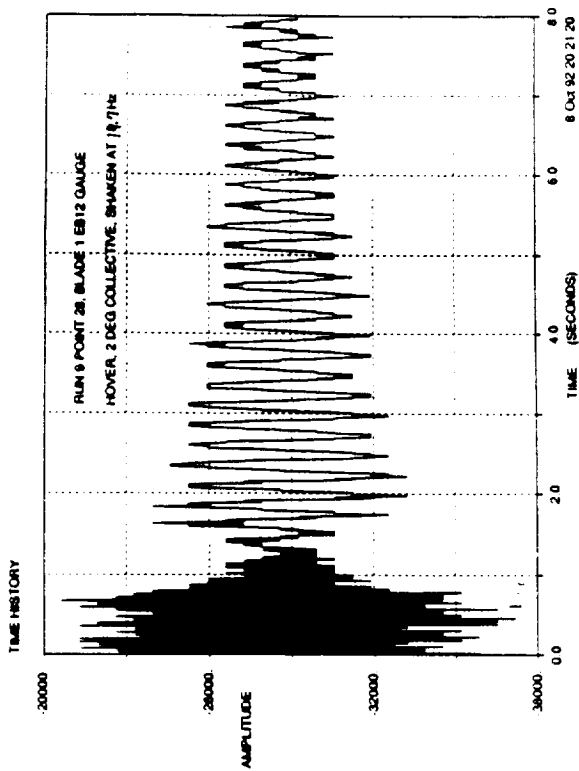


Fig. 24 Time history, FFT and Moving Block results from blade 1 edgewise bending strain gauge (FB1EB12) in the rotating frame. Shaken at the fixed frame 2L regressing lag frequency, 19.7 Hz. (Run 9, Point 28)

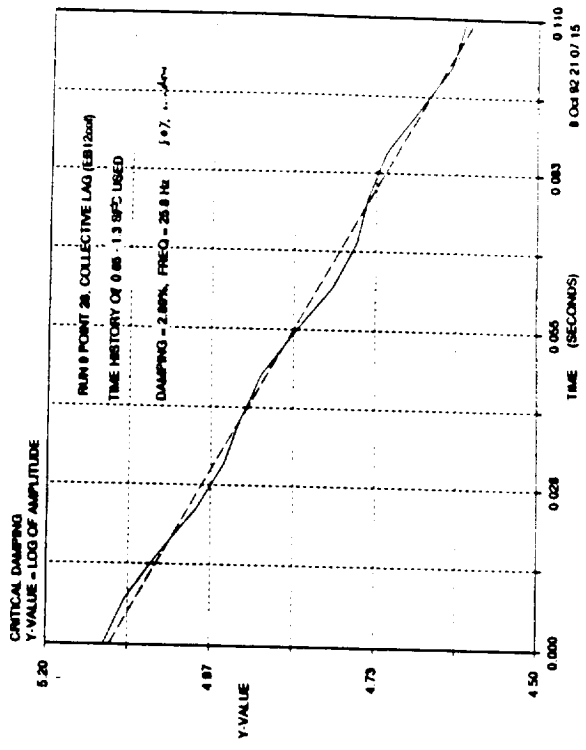
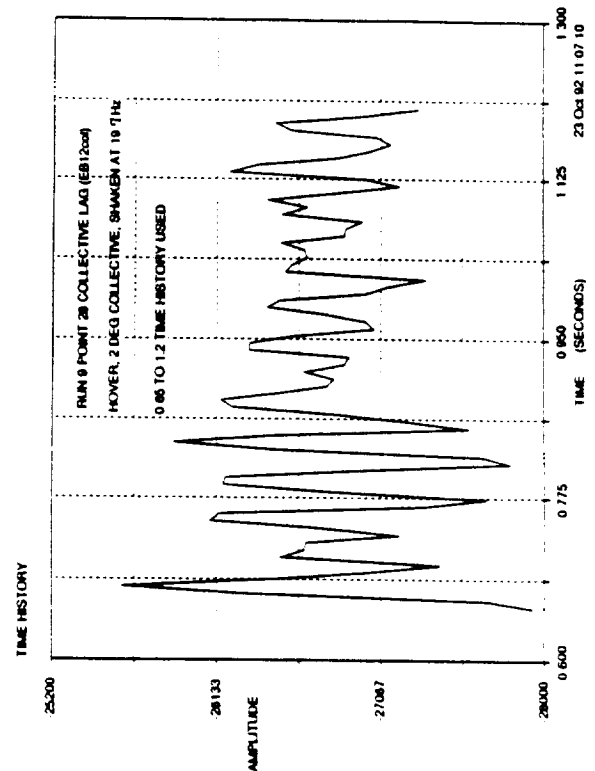
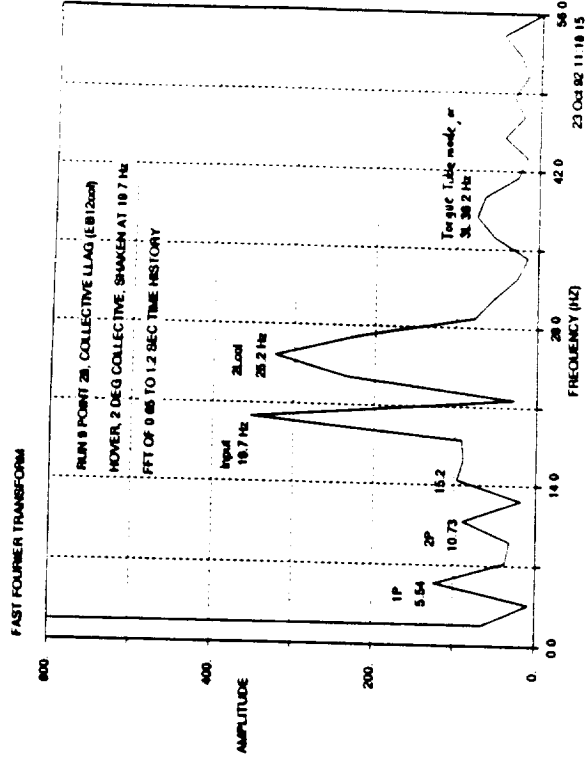
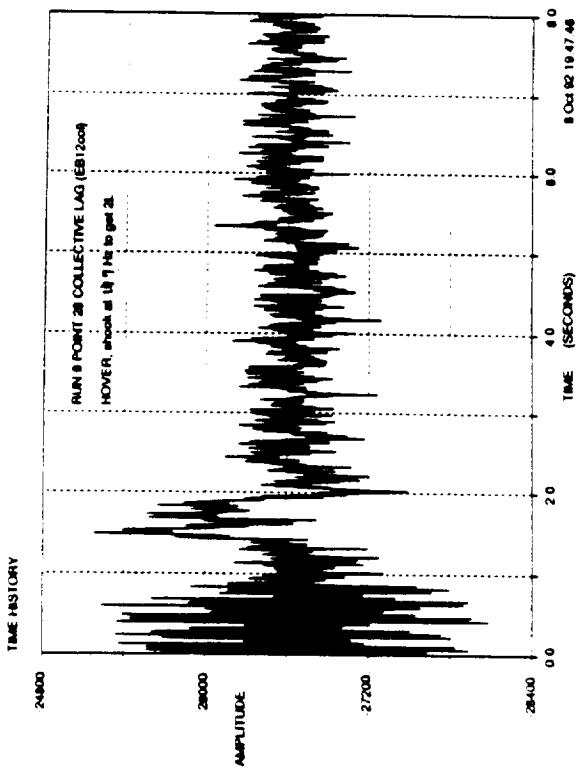


Fig. 25 Time history, FFT and Moving Block results from the 2nd lag mode collective component. Shaken at the fixed frame 2L regressing lag frequency, 19.7 Hz. (Run 9, Point 28)

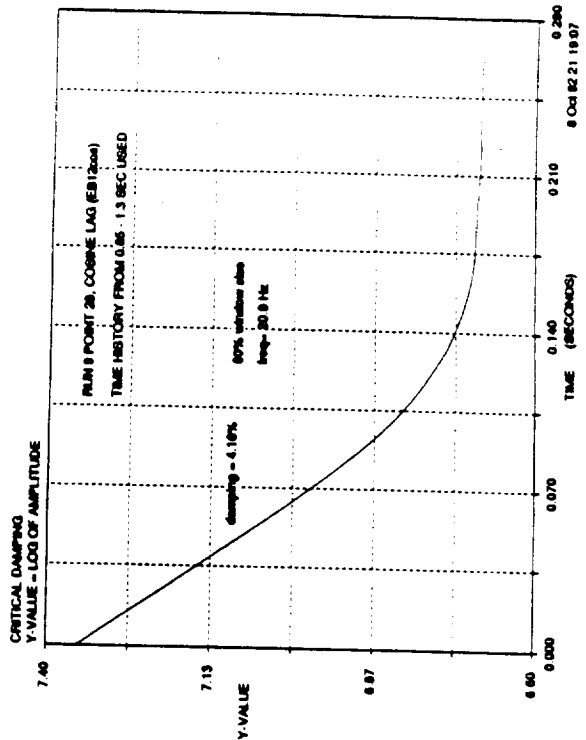
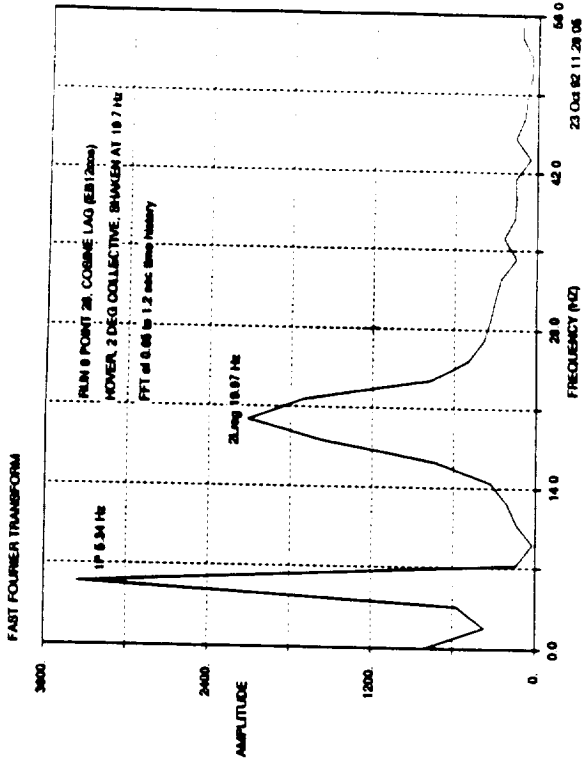
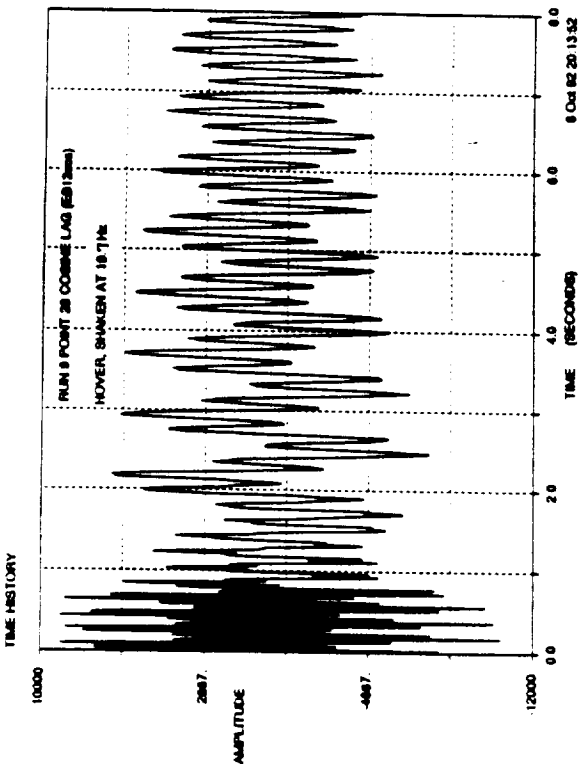


Fig. 26 Time history, FFT and Moving Block results from the 2nd lag mode cosine component. Shaken at the fixed frame 2L regressing lag frequency, 19.7 Hz. (Run 9, Point 28)

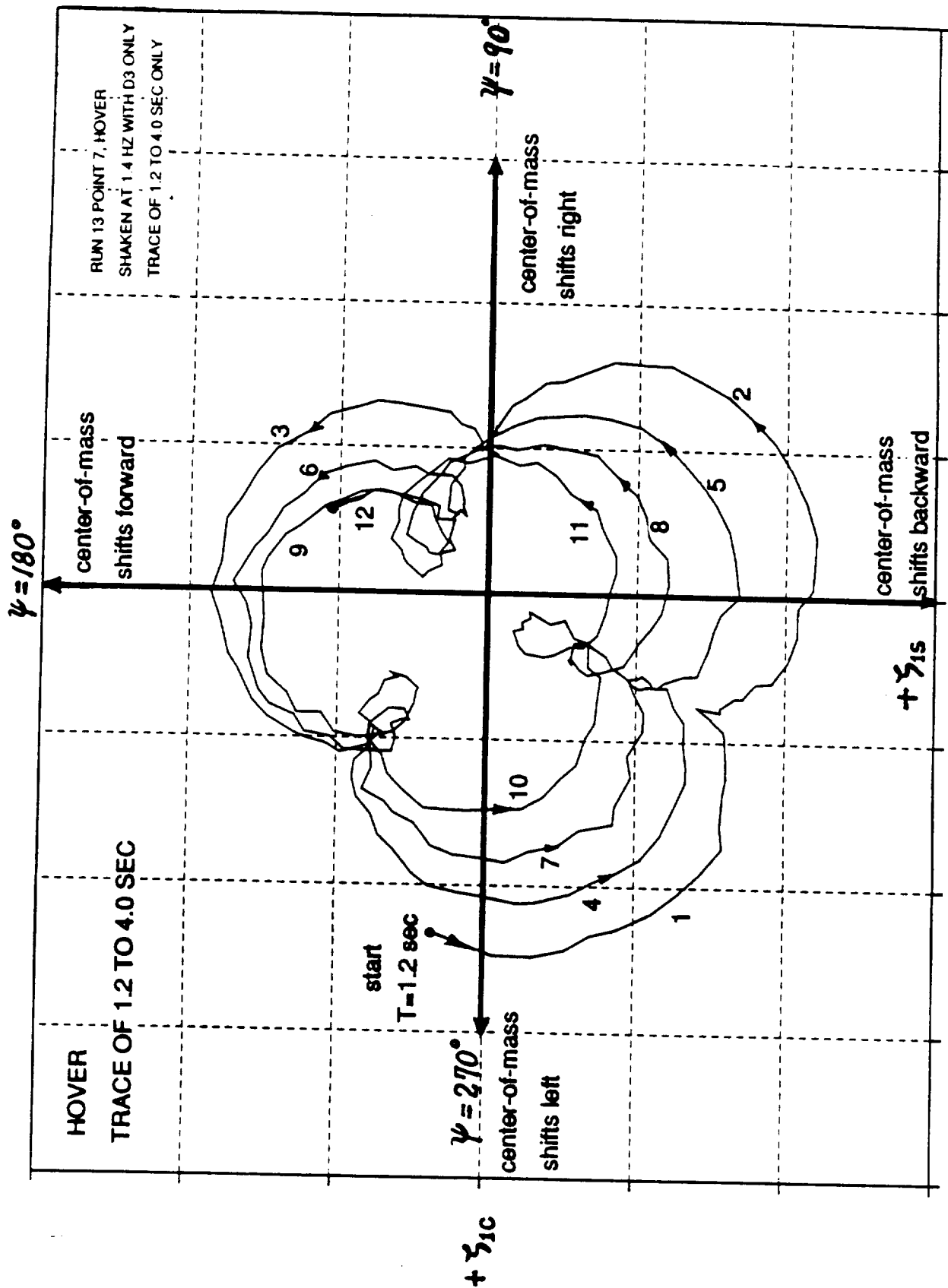


Fig. 27 Motion of the rotor center-of-mass for Run 13, Point 7, from 1.2 to 4 seconds. It is dominated by regressing lag motion.

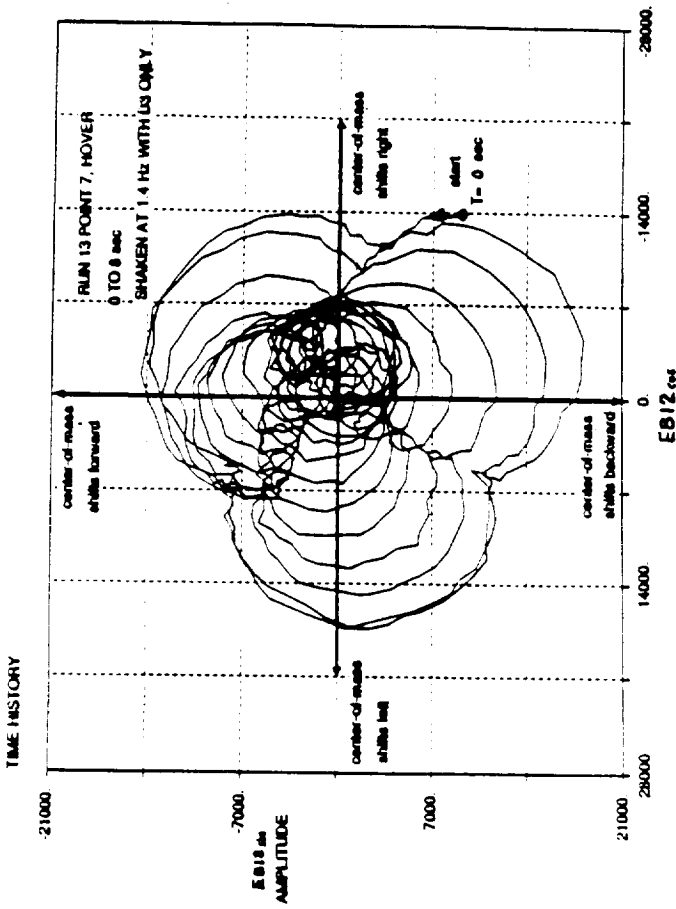


Fig. 28 Motion of the rotor center-of-mass for Run 13, Point 7, from 0 to 8 seconds. It is dominated by regressing lag motion.

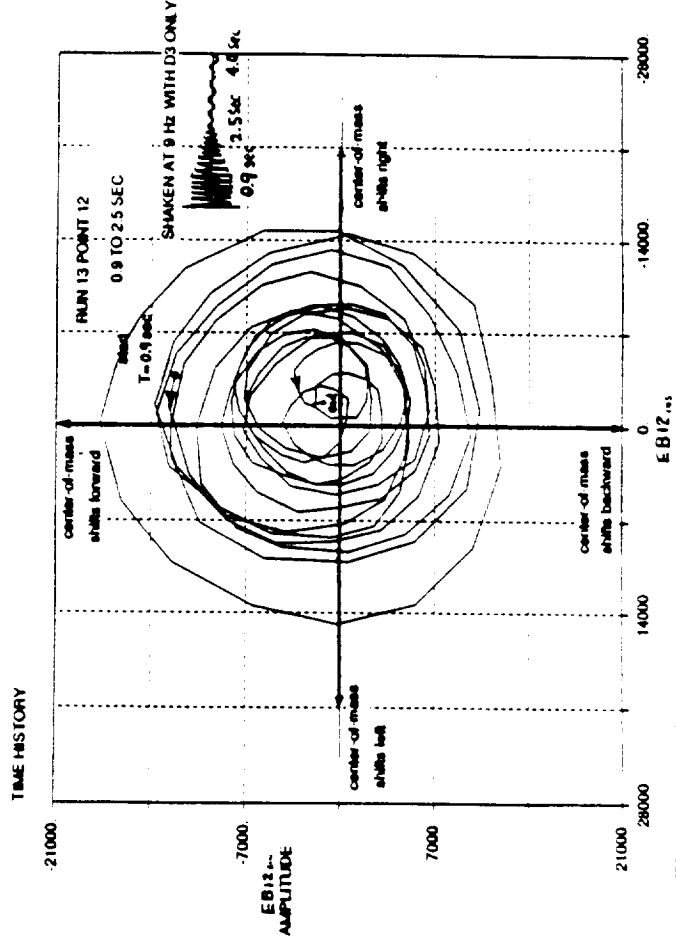


Fig. 30 Motion of the rotor center-of-mass for Run 13, Point 12, from 0.9 to 2.5 seconds. It is dominated by progressing lag motion.

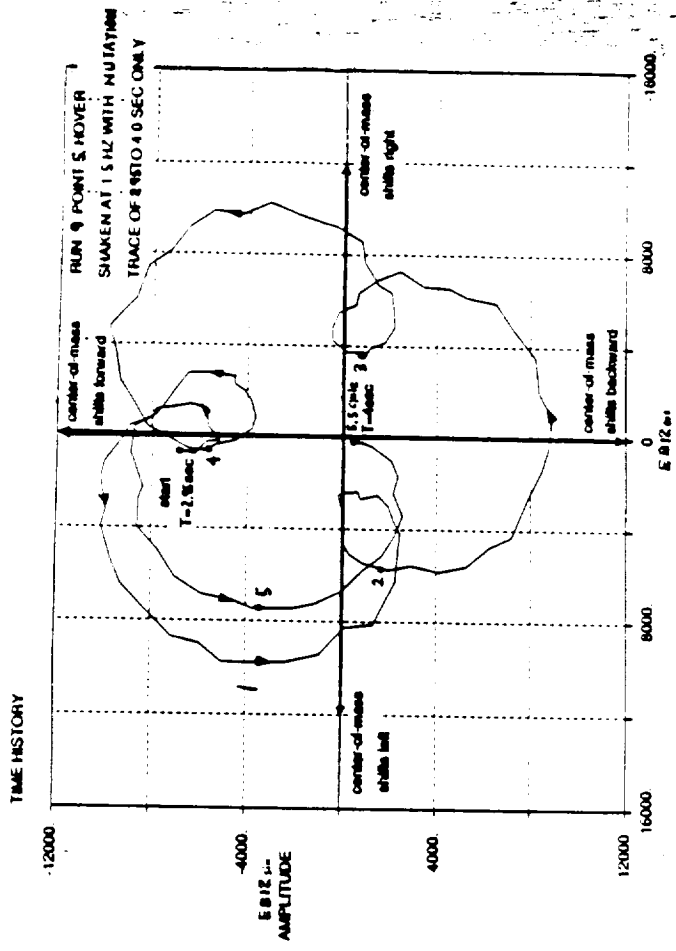


Fig. 29 Motion of the rotor center-of-mass for Run 9, Point 5, from 2.95 to 4 seconds. It is dominated by regressing lag motion.

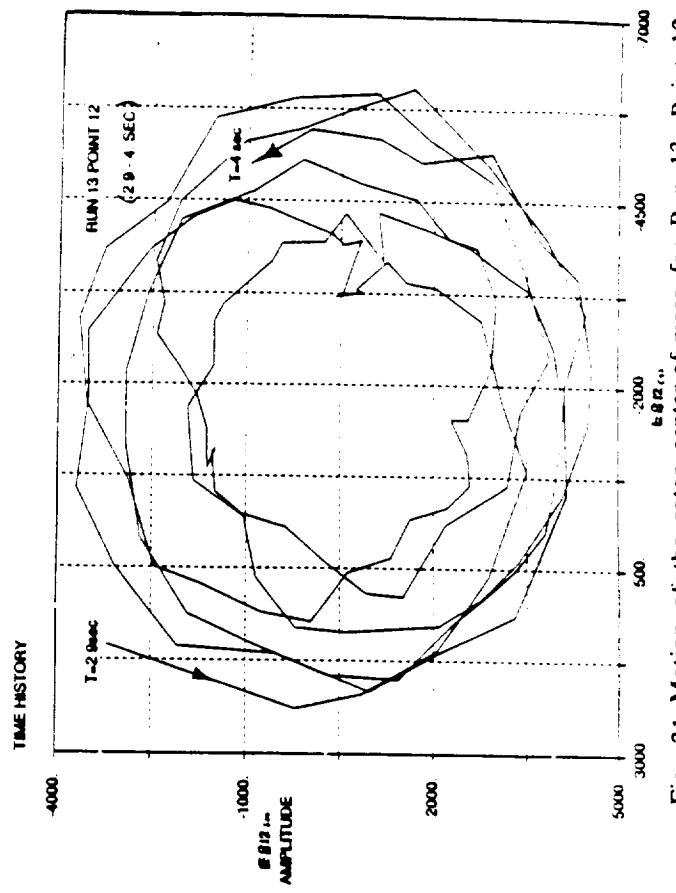


Fig. 31 Motion of the rotor center-of-mass for Run 13, Point 12, from 2.9 to 4 seconds. It is dominated by 1/rev lag motion.